Journal of Fluids and Structures 17 (2003) 57–96

JOURNAL OF FLUIDS AND STRUCTURES

www.elsevier.nl/locate/jnlabr/yjfls

Fluctuating lift on a circular cylinder: review and new measurements

C. Norberg*

Department of Heat and Power Engineering, Lund Institute of Technology, P.O. Box 118, SE-22100 Lund, Sweden

Received 15 September 2000; accepted 18 May 2002

Abstract

Apart from providing some new experimental data the paper reviews previous investigations concerning fluctuating lift acting on a stationary circular cylinder in cross-flow. In particular, effects of Reynolds number in the nominal case of an infinitely long and nonconfined cylinder in a smooth oncoming flow are discussed. The Reynolds number range covered is from about $\mathrm{Re} = 47$ to 2×10^5, i.e., from the onset of vortex shedding up to the end of the subcritical regime. At the beginning of the subcritical regime ($\mathrm{Re} \simeq 0.3 \times 10^3$) a spanwise correlation length of about 30 cylinder diameters is indicated, the correlation function being based on near-cylinder velocity fluctuations in outer parts of the separated shear layer. In between Reynolds numbers 1.6×10^3 and 20×10^3, an approximate 10-fold increase in the sectional r.m.s. lift coefficient is indicated. This range contains a fundamental change-over from one flow state to another, starting off at $\mathrm{Re} \simeq 5 \times 10^3$ and seemingly fully developed at $\mathrm{Re} \simeq 8 \times 10^3$.

1. Introduction

Flow around cylindrical structures is of relevance for many practical applications, e.g. offshore risers, bridge piers, periscopes, chimneys, towers, masts, stays, cables, antennae and wires. Knowledge about flow-related unsteady loading on such structures is crucial for hydro- and aerodynamic design and control (Blevins, 1990).

The present work will focus on the unsteady cross-stream force, the fluctuating lift, acting on a single circular cylinder in cross-flow. Under nominal conditions and when present, the fluctuating lift is dominated by the actions from the periodic phenomenon called vortex shedding, the principal source of cross-stream flow-induced vibration and acoustic emissions (Blake, 1986). The fluctuating lift is due mainly to the fluctuating pressures acting on the surface of the cylinder (Drescher, 1956; Kwon and Choi, 1996) and, except for the rearmost part of the cylinder, the pressure fluctuation energy is concentrated to a band around the mean shedding frequency f_S (Sonneville, 1976; Norberg, 1986). The alternate periodic shedding causes the pressure fluctuations at around f_S to be essentially out-of-phase between the upper and lower side of the cylinder (Gerrard, 1961; Ferguson and Parkinson, 1967), i.e., the lift fluctuation energy is concentrated to a band around f_S.

Obviously, the nondimensional shedding frequency, the Strouhal number

$$\mathrm{St} = \frac{f_S\, d}{U}, \tag{1}$$

*Corresponding author. Tel.: +46-46-2228606; fax: +46-46-2228612.
E-mail address: christoffer.norberg@vok.lth.se (C. Norberg).

0889-9746/03/$ - see front matter
PII: S0889-9746(02)00099-3

where d is the cylinder diameter and U is the free-stream velocity, has a special importance for the fluctuating lift. The appropriate Reynolds number in the assumed incompressible flow is

$$\mathrm{Re} = \frac{\rho U d}{\mu}, \tag{2}$$

where μ is the dynamic viscosity and ρ is the density of the fluid. The present paper will focus on Reynolds number effects for the nominal case of an "infinitely" long, rigid, smooth and unconfined cylinder in a uniform oncoming cross-flow, i.e., flow around a nonvibrating cylinder with negligible effects of surface roughness, with a large enough aspect ratio and with suitable end conditions (Williamson, 1989) at vanishing or very small solid blockage ratios (wall confinement) and free-stream turbulence, respectively. These additional factors have all been shown to have an influence on the flow in general and on the fluctuating lift in particular; e.g., see Farell (1981) and Blevins (1990) and references cited therein. In this work, the Reynolds number range of principal interest is from $\mathrm{Re} \simeq 47$ to 2×10^5, i.e., from the onset of vortex shedding up to the end of the subcritical regime where there is a rapid decrease in mean drag coefficient with increasing Re, the so-called drag crisis. For review on fluctuating loads at higher Re, see Farell (1981), Basu (1985) and Ribeiro (1992).

A compilation of St(Re) from selected experiments and two-dimensional (2-D) numerical simulations is shown in Fig. 1. Smoke-wire flow visualizations (Norberg, 1992, 1993a) reveal that the change-over to a low-quality shedding frequency at $\mathrm{Re} \simeq 5.1 \times 10^3$ is associated with a transitional change in the three-dimensionality of near-wake vortex shedding, more specifically with an increasing degree of spanwise waviness of primary vortices and by the (somewhat later) inception of naturally occurring and random-positioned vortex dislocations; see also Prasad and Williamson (1997b) and Section 6.3.2.

The amplitudes of fluctuating drag, which are significantly smaller than the fluctuating lift (Bouak and Lemay, 1998; Posdziech and Grundmann, 2000), are dominated by fluctuating pressures that are in-phase between the upper and lower side of the cylinder, which in turn are concentrated to very low frequencies and to a band around two times f_S (Sonneville, 1976). Due mainly to vortex shedding, basically as an effect of frictional forces, the cylinder also experiences a fluctuating torque around its axis. Even for relatively low Reynolds numbers in the laminar shedding regime ($\mathrm{Re} \simeq 47$ to 190), the fluctuating torque appears to be of minor importance (Jordan and Fromm, 1972; Lecointe and Piquet, 1989).

The r.m.s. (root-mean-square) lift coefficient is defined as

$$C_{L'} = \frac{L'}{d\ell_c \rho U^2/2}, \tag{3}$$

where L' is the r.m.s. of lift fluctuations acting on a spanwise segment of length ℓ_c (lift is assumed to have a zero time-mean value). The *sectional* r.m.s. lift coefficient is the r.m.s. lift coefficient for which the segment length is vanishingly small ($\ell_c/d \to 0$). The sectional lift can thus be seen as lift per unit span. The *total* lift fluctuations are defined as those acting on the whole cylinder length exposed to flow ($\ell_c = \ell$).

The very first measurement of fluctuating lift on a circular cylinder in a continuous[1] fluid stream was carried out by Drescher (1956), who recorded the sectional wall pressure distribution around the cylinder as a function of time in a flow of water for $\mathrm{Re} = 1.1 \times 10^5$. Since this pioneering work, a vast amount of quantitative data has been reported and numerous compilation graphs on the variation of lift-related coefficients with Reynolds number have been presented, e.g. Morkovin (1964), Lienhard (1966), Norberg (1987b), Blevins (1990), Ribeiro (1992), West and Apelt (1993) and Blackburn and Melbourne (1996). Despite these efforts, there has been no real consensus on $C_{L'}(\mathrm{Re})$, in particular for $\mathrm{Re} < 6 \times 10^3$. As for the collected data on fluctuating forces, especially r.m.s. lift, the range from about $\mathrm{Re} = 190$ (the approximate onset of intrinsic three-dimensional flow) to $\mathrm{Re} \simeq 6 \times 10^3$ has been greatly overlooked in the past. This gap of knowledge reflects some basic difficulties encountered in numerical simulations and related laboratory experiments; reliable numerical simulations for Re greater than about 190 must be carried out with very fine temporal/spatial resolutions and in a relatively large three-dimensional domain (Zhang et al., 1995)—laboratory experiments for Re less than about 6×10^3 often require small cross-stream dimensions (Keefe, 1961) with the necessity of rather large spanwise aspect ratios, ℓ/d (West and Apelt, 1982; Norberg, 1994). Another complicating factor is the instrumentation of the

[1] In Schwabe (1935) instantaneous pressure distributions around a cylinder in accelerating motion are estimated from the unsteady Bernoulli equation using velocities as determined from photographs of streamlines in water. At an instant when the cylinder is shedding vortices, the Reynolds number being 735 and still increasing, Schwabe finds a sectional lift coefficient of 0.447 and a drag coefficient of 1.09. The unsteady force measurements by Bingham et al. (1952) are carried out in a shock tube, covering only a few shedding cycles after the shedding is initiated by a shock wave, at a single combination of Mach and Reynolds number ($\mathrm{Ma} = 0.4$, $\mathrm{Re} = 77 \times 10^3$). The pressure variations around a section of the cylinder, as deduced from density variations using a Mach–Zehnder interferometer assuming two-dimensional flow, is reported to build up lift oscillation amplitudes of $C_L \sim 0.9$.

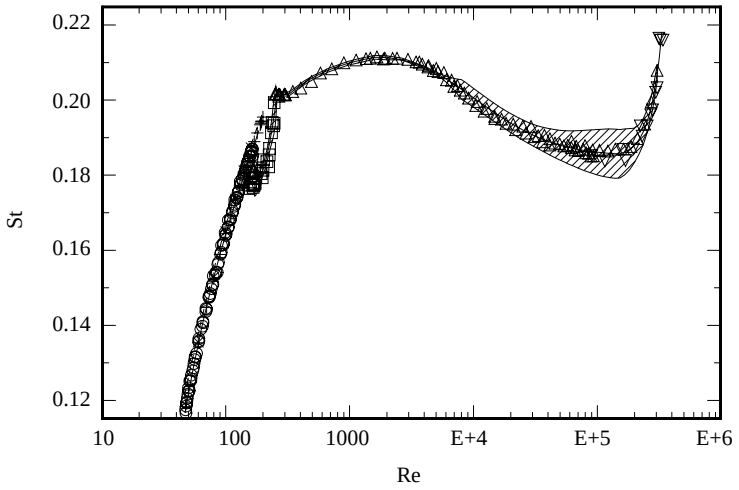

Fig. 1. Strouhal number versus Reynolds number: ▽, Bearman (1969); Norberg (1987a, 1994): ○, laminar shedding; □, wake transition; △, turbulent shedding; ---, Barkley and Henderson (1996), 2-D; ×, Kwon and Choi (1996), 2-D; +, Posdziech and Grundmann (2000), 2-D; ——, formulas in Appendix A. Shaded region corresponds to the bandwidth (−3 dB) of the shedding peak frequency.

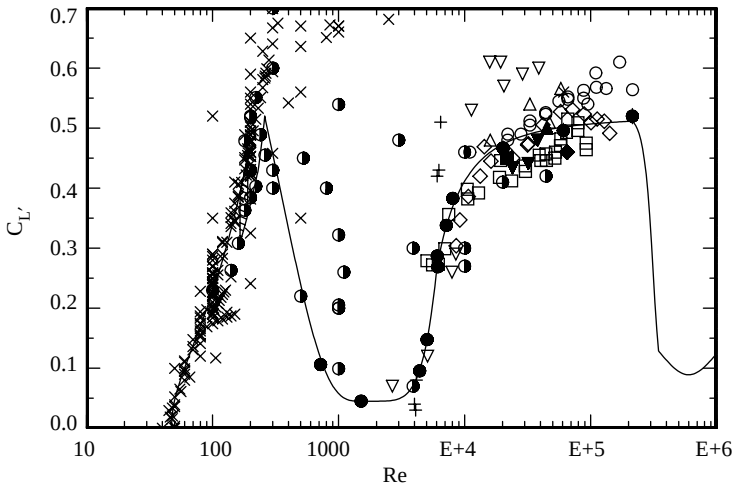

Fig. 2. R.m.s. lift coefficient versus Reynolds number: □, Keefe (1962); +, Leehey and Hanson (1971); ▲, Sonneville (1973); △, Mohr (1981); ▽, Moeller and Leehey (1984); ▩, Gartshore (1984); ◇, Szepessy and Bearman (1992); ○, West and Apelt (1993); ◆, Sakamoto and Haniu (1994); ×, 2-D; half-filled circle, 3-D; ●, present; ——, formulas in Appendix A.

cylinder; the sectional lift force has to be sensed on a short segment of the cylinder span and the necessary space required for sufficiently sensitive force and/or pressure transducers sets a lower practical limit to the cross-stream dimension (Moeller, 1982). A review on measurement (laboratory) methods is provided in Section 3. Appendix B contains a short review on numerical simulations.

In 1992, the author presented experimental data on the sectional r.m.s. lift coefficient for Reynolds numbers between 720 and 2×10^5 (Norberg, 1993a). These coefficients are based on measurements of fluctuating wall pressures at the shoulders of the cylinder and are calculated using a formula proposed by Ribeiro (1991). Since then, the reliability of this data has been further consolidated (Apelt and West, 1996). In addition, the above-mentioned gap of information has been partly filled out by data from numerical three-dimensional (3-D) simulations, e.g. Beaudan and Moin (1994), Zhang et al. (1995), Kravchenko et al. (1999) and Evangelinos and Karniadakis (1999); see also Table 6.

A compilation on $C_{L'}$ versus Re is shown in Fig. 2. The experimental data in Fig. 2 only contain sectional or near-sectional lift coefficients ($\ell_c/d \leqslant 1$). The free-stream turbulence levels are all less than Tu = 0.2%, except those of

Table 1
Measurements of fluctuating lift ($Re < 3 \times 10^5$, $Tu \leqslant 2\%$)

Study	$Re/10^4$	β(%)	ℓ/d	ℓ_c/d	Tu(%)	EP[a]	M[b]	F[c]	$C_{L'}$[d]
Drescher (1956)	11	24	3.1	sec.	?	–	P1	w	≈0.8
Fujino et al. (1958)	8–60	?	7.0	Tot.	–	–	F2	w	≈0.06–0.3
McGregor and Etkin (1958)	4–12	2.6	28	Sec.	0.3	–	P4	a	0.41–0.42
Macovsky (1958)	2–10	8.3	12	2.0	–	–	F1	w	≈0.2–0.7
Fung (1960)	19–139	10.5	5.7	1.7	?	–	F1	a	0.14–0.27
Humphreys (1960)	3–57	16	6.6	Tot.	1.0	–	F2	a	≈0.2–0.5
Weaver (1961)	8–36	≃6	≃10	Tot.	0.5	x	F2	a	≈0.1–0.2
Gerrard (1961)	0.4–18	1–15	7–80	Sec.	0.3	–	P4	a	0.02–0.87
Keefe (1962)	0.5–9.2	2.6	18[e]	1.0	0.3	x	F1	a	0.27–0.52
Bishop and Hassan (1964)	0.4–11	8.4	9.0[e]	3.0	?	x	F1	w	≈0.3–0.5
Ferguson and Parkinson (1967)	1.5–4	8.3	9.0	Sec.	0.1	–	P4	a	0.22–0.32
Protos et al. (1968)	4.5	5?	11	Tot.	?	–	F2	w	0.28
Feng (1968)	1.8/2.0	8.3	9.0	Sec.	0.1	–	P4	a	0.34/0.36
Leehey and Hanson (1971)	0.4–0.6	Open	97	Sec.	0.04	–	F3	a	0.03–0.51
Bublitz (1972)	10–66	Open	8.0	Tot.	0.3[e]	–	F2	a	0.02–0.07
Batham (1973)	11/24	5.0	6.6	Sec.	0.5[e]	–	P3	a	0.33/0.09
Tanida et al. (1973)	0.006–0.011	4.3	10	3.3	–	–	F1	o	0.03–0.09
Tanida et al. (1973)	0.3–0.8	4.3	10	3.3	–	–	F1	w	0.05–0.08
Sonneville (1973)	4.5	5.6	13	Sec.	0.4	–	P3	a	0.50
Kacker et al. (1974)	1–30	4.7	8.0	3.6[e]	≃0.4	–	F1	a	0.17–0.45
Kacker et al. (1974)	2.5–21	8.3	4.5	Sec.	≃0.4	–	P4	a	0.16–0.45
Huthloff (1975)	1–10	Open	6.2	Tot.	?	x	F2	a	0.25–0.42
Sonneville (1976)	1–6	5.6	13	Tot.	0.4	–	F2	a	0.33–0.51
Richter and Naudascher (1976)	2–30	17[e]	8.6	6.8	0.5	–	F1	a	0.04–0.92
Howell and Novak (1979)	7.5	?	5.8	Tot.	?[e]	–	F2	a	0.12
So and Savkar (1981)	3–51	32/16	4/8	3.0	0.5	–	F1	w	0.13–1.04
Mohr (1981)	1.5–5.5	9.5	24	Sec.	1.0	–	P1	a	0.47–0.56
Moeller (1982)	0.5–5.6	Open	16/19	0.4/0.5	0.3[e]	x	F1	a	0.17–0.53
Kiya et al. (1982)	3.2	9.1	11	Sec.	1.4[e]	–	P5	a	0.60
Schewe (1983)	2–710	10	10	Tot.	0.4	–	F2	a	0.01–0.38
Cheung and Melbourne (1983)	6–60	11/8	3.6/6.7	Tot.	0.4[e]	x	F2	a	0.04–0.46
Bychov and Kovalenko (1983)	15–70	15	6.7	1.7	0.04[e]	–	F1	a	≈0.02–0.1
Mulcahy (1983)	2–21	8.3	12[e]	3.0	2	x	F1	w	0.13–0.25
Mulcahy (1984)	2–18	8.3	7.5	0.5	1–2[e]	x	F1	w	0.21–0.50
Moeller and Leehey (1984)	0.3–3.9	3.1	26	0.5	0.9	x	F1	w	0.07–0.61
Gartshore (1984)	2.2	8.3	10	Sec.	0.1[e]	x	P2	a	0.45
Norberg (1986)	2.7	8.3	8.0	Sec.	0.1[e]	x	P6	a	0.57
Norberg and Sundén (1987)	1.8–30	4/11	12/8.8	Sec.	0.06[e]	x	P5	a	0.39–0.76
Sin and So (1987)	4.8	18	2.5	0.25	1.5	–	F1	a	1.24
Baban et al. (1989)	4.6	22.3	3.0	0.24	2.0	–	F1	a	0.82
Kiya and Tamura (1989)	≃4	Open	6.7	1.0	≃0.7	x	F1	a	0.38
Taniguchi and Miyakoshi (1990)	9.4	7.1	14	1.2	0.2	–	F1	a	0.38
Szepessy and Bearman (1992)	0.9–14	7.7	6.7[e]	Sec.	0.05	x	P2	a	0.30–0.53
Norberg (1993a)	0.07–21	1–11	9–105	Sec.	0.06	x	P7	a	0.04–0.56
West and Apelt (1993)	1.1–22	4–10	15–35	Sec.	0.2[e]	x	P1	a	0.46–0.61
Sakamoto and Haniu (1994)	6.5	8.2	8.2	0.92	0.2	–	F1	a	0.46
Blackburn and Melbourne (1996)	12–60	10	4.5	0.1	0.6[e]	x	F1	a	0.13–0.96
Watanabe et al. (1996)	11–44	9.8	3.3	Tot.	0.1	–	F2	w	0.06–0.51
Khalak and Williamson (1996)	0.2–1.3	10	10	Tot.	0.9	(x)	F2	w	0.03–0.30
Bouak and Lemay (1998)	2.4–3.8	3.3	33	1.0	0.2	x	F1	a	0.44–0.48

[a] Indicator whether end plates are used.
[b] Classification of measurement method, see Section 3.3.
[c] Fluid (a: air, w: water, o: oil).
[d] ≈ implies that r.m.s.-values have been estimated.
[e] Reference contains a separate study on the influence of this parameter.

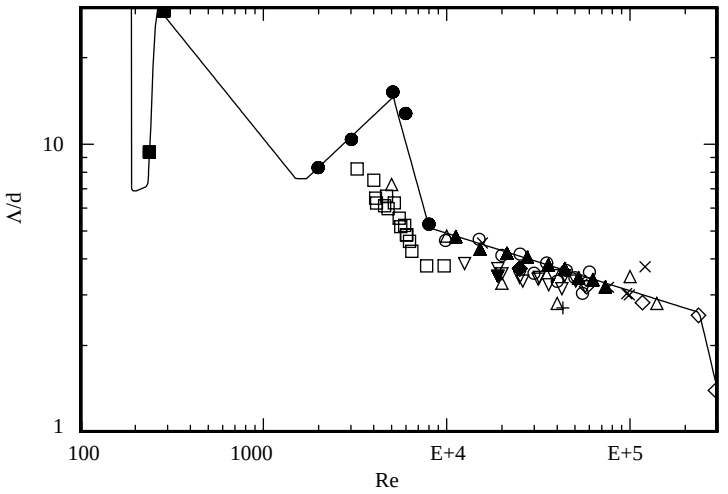

Fig. 3. Normalized spanwise correlation length versus Reynolds number: □, Leehey and Hanson (1971); ♦, Bearman and Wadcock (1973); ×, Kacker et al. (1974); ◇, Bruun and Davies (1975); ○, Sonneville (1976); ▼, Novak and Tanaka (1977); ▽, Moeller (1982); +, Szepessy (1994); △, Iida et al. (1997); ▩, $d = 3$ mm; ●, $d = 6$ mm; ▲, $d = 40$ mm; ——, formulas in Appendix A.

Moeller and Leehey (1984) (Tu = 0.9%) and Mohr (1981) (Tu = 1.0%). A summary of previous laboratory measurements of both sectional and total lift fluctuations, for $\mathrm{Re} < 3 \times 10^5$ and $\mathrm{Tu} \leqslant 2\%$, is found in Table 1; numerical simulations (2-D/3-D) are summarized in Appendix B.

The fluctuating lift on a finite cylinder segment is dependent on the degree of three-dimensionality in the shedding flow close to the cylinder. One measure of this three-dimensionality is the spanwise or axial correlation length scaled with the diameter, Λ/d (Section 2.1). The scarceness of data for this quantity is even larger than for the r.m.s. lift coefficient (Ribeiro, 1992). In fact, up to now, there are no reliable measurements of Λ/d for $\mathrm{Re} < 2 \times 10^3$. In an attempt to bridge this gap of information, a near-wake spanwise correlation study was carried out, extending down to Re = 230 and using hot-wire anemometry (Section 5.2).

Knowledge of spanwise correlation also has a great significance for vortex-induced sound generation (Æ olian tones) and for the important question of the necessary spanwise computational dimension to capture significant flow-dynamic features in 3-D numerical simulations. A compilation of Λ/d versus Re with data from previous investigations together with present results is shown in Fig. 3. As before, the solid line refers to empirical formulas (Appendix A). For turbulent shedding conditions ($\mathrm{Re} > 260-300$) and with increasing Re there is a general downward trend in Λ/d versus Re. However, there is a local maximum at $\mathrm{Re} \simeq 5 \times 10^3$, previously noted by Norberg (1987a); see also Section 5.3, which coincides with the Reynolds number with inception of low-spectral-quality shedding (Fig. 1). The critical value of $\mathrm{Re} \simeq 5 \times 10^3$ has been suggested in Norberg (1998) to be due to a spanwise resonance phenomenon in between vortical structures of mode B (Williamson, 1988b, 1996b) and shear-layer vortices (Bloor, 1964; Wu et al., 1996).

The main objective of this work is to make an overview of the fluctuating lift acting on a circular cylinder, especially regarding the influence of Reynolds number and the relation between fluctuating lift and flow features in the near-wake region.

2. Fluctuating lift

The unsteady force on a segment having a finite spanwise (axial) length ℓ_c is the integrated result from a temporal–spatial loading on that section. The time-averaged flow is assumed to be homogeneous in the spanwise direction, at least within a significant central spanwise region. This central flow is supposed to be two-dimensional in the mean sense and also independent of the actual spanwise length ℓ of the cylinder, i.e., independent of the aspect ratio ℓ/d. In laminar shedding flows this might require some slight end modifications, see Williamson (1996a) for a review. At higher Reynolds numbers, in transitional and turbulent shedding flows, the necessary minimum aspect ratio varies with Reynolds number which in turn also, at least to some extent, is dependent on the end conditions (West and Apelt, 1982; Szepessy and Bearman, 1992; Szepessy, 1993; Norberg, 1994). In Keefe (1962) and Szepessy and Bearman (1992), using

end plates, a decrease in aspect ratio below about $\ell/d = 10$ for $\mathrm{Re} = 10^4$ and below about $\ell/d = 6$ for $\mathrm{Re} = 10^5$ increases the (sectional) r.m.s. lift. From the study of aspect-ratio effects by the author (Norberg, 1994) it is to be noted that for $\mathrm{Re} < 8 \times 10^3$, approximately, and when using end plates, the mean pressure loading is reduced with a decrease in aspect ratio while the opposite is true for higher Re. As mean and fluctuating loads are interconnected (Farell, 1981) this implies that the effect of aspect ratio on r.m.s. lift changes its behavior at $\mathrm{Re} \simeq 8 \times 10^3$.

2.1. Sectional lift and axial correlation

In transitional and turbulent shedding flows, the vortex shedding does not occur in phase over the whole span (as it does or can be made to do in laminar shedding flows). Thus, the correlation or coherence between two sectional fluctuating forces separated a certain spanwise distance, s, decreases with increasing s. This means that the sectional r.m.s. lift coefficient is always greater than or equal to the finite section r.m.s. lift coefficient. Assuming spanwise homogeneity, the ratio, γ_L, between the r.m.s. lift on a finite length ℓ_c and the sectional r.m.s. lift times ℓ_c is (Kacker et al., 1974)

$$\gamma_L = \frac{1}{\ell_c}\left[2\int_0^{\ell_c} (\ell_c - s)\, R_{LL}(s)\, \mathrm{d}s\right]^{1/2}, \tag{4}$$

where $R_{LL}(s)$ is the correlation coefficient, at zero time delay, between sectional lift forces separated a spanwise distance s. Since lift is dominated by actions of surface wall pressures, an accurate approximation for R_{LL} is the lift correlation based on sectional pressure forces, for which measurements are provided in West and Apelt (1997). Measurements of R_{LL} from sectional total forces by Blackburn and Melbourne (1996) support this approximation. As discussed in Ribeiro (1992), also see Sonneville (1976) and Moeller (1982), the correlation coefficient, $R_{pp}(s)$, between fluctuating wall pressures along the generator at $\varphi = 90^\circ$ (the mean stagnation line is at $\varphi = 0^\circ$) or between fluctuating velocities along a generator close to the separated shear layers but not too far from the cylinder, $R_{uu}(s)$, can also provide a reasonable estimate for R_{LL}, i.e., $R_{LL}(s) \approx R_{pp}(s) \approx R_{uu}(s)$. Thus, with a known or estimated correlation function R_{LL}, Eq. (4) can be used to convert the finite section r.m.s. lift coefficient to the sectional r.m.s. lift coefficient.

The one-sided spanwise correlation length Λ and the centroid of spanwise correlation σ, related to the fluctuating lift, are defined as (Blake, 1986)

$$\Lambda = \int_0^{\infty} R_{LL}(s)\, \mathrm{d}s, \tag{5}$$

$$\sigma = \Lambda^{-1} \int_0^{\infty} s\, R_{LL}(s)\, \mathrm{d}s. \tag{6}$$

At large separations and for turbulent shedding conditions R_{LL} is expected to vanish, $R_{LL}(s \to \infty) = 0$. In reality, the upper limits in Eqs. (5,6) have to be finite and for convenience, neglecting effects of end disturbances, they can be set to the full length of the cylinder. A neglect of end disturbances implies a sufficiently large aspect ratio, and under such circumstances and when the segment length ℓ_c equals the full length ℓ in Eq. (4) the lift ratio becomes (Keefe, 1961)

$$\hat{\gamma}_L = \ell^{-1} \sqrt{2\Lambda(\ell - \sigma)}. \tag{7}$$

This is the ratio between the total r.m.s. lift coefficient and its sectional counterpart. Naturally, $\hat{\gamma}_L$ equals unity in fully correlated flow ($\Lambda = \ell$, $\sigma = \ell/2$).

The simplest model function for R_{LL} is the exponential decay,

$$f_1 = \exp(-s/\Lambda_1). \tag{8}$$

The centroid for the exponential decay is equal to the correlation length, $\sigma_1 = \Lambda_1$. The associated lift ratio is (Loiseau and Szechenyi, 1972)

$$\gamma_{L_1} = \frac{\sqrt{2}}{a}[\exp(-a) + a - 1]^{1/2}, \tag{9}$$

where $a = \ell_c/\Lambda_1$. The ratio γ_{L_1} equals 0.99 when ℓ_c occupies 6% of the correlation length ($a = 0.06$). Present results (Section 5.3) indicated that the exponential decay is a reasonable approximation for $\mathrm{Re} \geqslant 8 \times 10^3$; see also ESDU (1985). As an example, $\Lambda \simeq \Lambda_1 \simeq 5\,d$ prevails at $\mathrm{Re} = 10^4$ (Fig. 3), i.e., a segment with $\ell_c = d$ (e.g. Keefe, 1961) produces a r.m.s. lift coefficient that is about 3% lower than its sectional counterpart.

Another model function for R_{LL} is

$$f_2 = \left[1 + \left(\frac{s}{C\Lambda_2}\right)^n\right]^{-1}. \tag{10}$$

For each exponent $n > 1$ in Eq. (10) the constant C is determined from

$$C = \frac{n}{\pi}\sin\frac{\pi}{n}. \tag{11}$$

A finite centroid in the limit $s \to \infty$ requires $n > 2$. The ratio between the centroid and the correlation length then is

$$\sigma_2/\Lambda_2 = C\frac{\sin(\pi/n)}{\sin(2\pi/n)}. \tag{12}$$

In cases when either f_1 or f_2 works as an approximation the following weighted combination can be tested ($0 \leqslant \alpha \leqslant 1$):

$$R_{LL} = (1-\alpha)f_1 + \alpha f_2. \tag{13}$$

Using this weighted model, Λ and σ can be calculated from

$$\Lambda = (1-\alpha)\Lambda_1 + \alpha\Lambda_2, \sigma = [(1-\alpha)\Lambda_1^2 + \alpha\Lambda_2\sigma_2]/\Lambda. \tag{14, 15}$$

Eq. (13) was used as a model for present results, using $R_{LL} \approx R_{uu}$ as an approximation (Section 5.3).

2.2. Relations to flow-induced sound and vibration

If vortex shedding is assumed to be an essentially sinusoidal process, the sectional lift force may be modelled as a time-harmonic function, i.e.,

$$C_L(t) = \sqrt{2}C_{L'}\sin(2\pi f_S t).$$

Now assume that the lift force acts on a spring-mounted (natural frequency f_n), linearly damped (structural damping factor ζ), rigid cylinder (mass m, including added mass) of length ℓ. The cylinder is restrained to move only in the lift direction and the vibration is assumed to be sinusoidal with an amplitude A, at a frequency equal to f_n. With this simple harmonic model (adopted from Blevins, 1990) the amplitude is largest at resonance, i.e., for $f_S = f_n$. The scaled r.m.s. amplitude then is

$$\left(\frac{A'}{d}\right)_{f_S=f_n} = \frac{\hat{\gamma}_L C_{L'}}{4\pi \mathrm{St}^2 \delta_r},$$

where $\hat{\gamma}_L$ is the total lift ratio from Eq. (7) and $\delta_r = 4\pi m\zeta/(\rho\ell d^2)$ is the reduced damping. Complications to the above simple model are that relatively small amplitudes of vibration might increase the spanwise coherence of shedding vortices (Toebes, 1969; Novak and Tanaka, 1977), the vortex strength (Davies, 1976) and thus also the sectional (and total) r.m.s. lift (Ferguson and Parkinson, 1967; King, 1977). Increasing vibration amplitudes may also increase the ability for a synchronization or lock-in of the shedding to the vibration frequency (Bishop and Hassan, 1964). Calculation procedures including extensions to take into account synchronization and feedback between motion and forces are presented in ESDU (1985). The limiting amplitude for the above simple analysis to be valid is probably very small, of the order some percent of the cylinder diameter. Nevertheless, it is obvious that detailed information on sectional fluctuating lift and its associated spanwise correlation is essential for the prediction of low-amplitude transverse vortex-induced vibration. It should also be noted that more advanced models for vortex-induced vibration normally include sectional lift and correlation data for the stationary cylinder, e.g., see Vickery and Basu (1983), Blevins (1990) and Skop and Balusubramanian (1997).

A theory for the sound emitted from a non-vibrating cylinder with partially correlated vortex shedding is presented in Phillips (1956); see also Blevins (1990). Under the assumptions of a sinusoidal fluctuating lift, a cylinder length much shorter than the sound wavelength ($\ell \ll \lambda$) but longer than the centroid ($\ell > \sigma$), the r.m.s. sound pressure at a distance $r \gg \lambda$ along a line in the lift direction is

$$p'_s = \sqrt{\overline{p_s^2}} = \frac{\rho U^2}{4}\left(\frac{\ell}{r}\right)\mathrm{Ma}\hat{\gamma}_L C_{L'}\mathrm{St},$$

where $C_{L'}$ is the sectional r.m.s. lift coefficient (Ma is the Mach number which is small, as the flow is assumed to be incompressible). The lift-generated sound has a dipole character, with dipole axis normal to the stream (Gerrard, 1955;

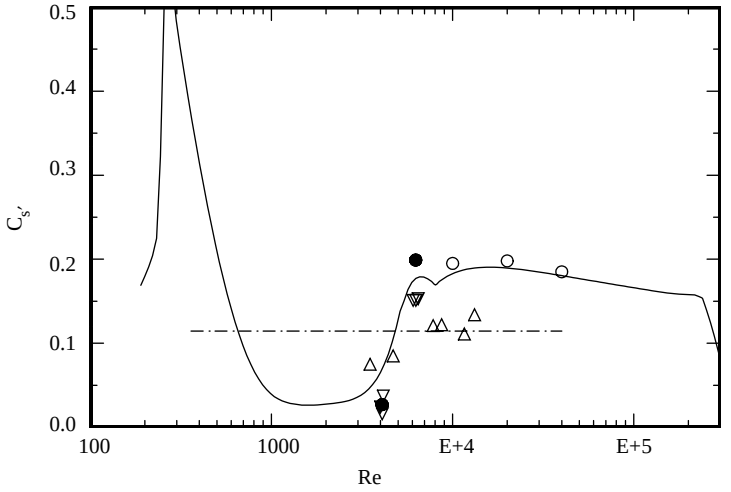

Fig. 4. R.m.s. sound pressure coefficient versus Reynolds number: dotted line, Phillips (1956), sound; △, Keefe (1961), sound; ●, Leehey and Hanson (1971), lift; ▽, Leehey and Hanson (1971), sound; ○, Iida et al. (1997), sound; ——, present, lift (based on formulas in Appendix A).

Etkin et al., 1956). Following Keefe (1961), a convenient r.m.s. sound pressure coefficient is

$$C_{s'} = \frac{2\sqrt{2}p'_s r}{\rho U^2 \mathrm{Ma}\sqrt{d(\ell-\sigma)}} = C_{L'}\mathrm{St}\sqrt{\Lambda/d}. \tag{16}$$

As indicated in Section 2.1, the centroid σ is of the same order as the correlation length Λ. In turbulent shedding flows $\ell \gg \sigma$ often prevails, e.g., for telephone wires in natural wind, which means that the radiated power intensity ($\propto \overline{p_s^2}$) then is directly proportional to the cylinder length. Obviously, the combination quantity $C_{L'}\,\mathrm{St}\sqrt{\Lambda/d}$ is of special significance for vortex-induced sound from stationary cylinders (Æ olian tones). Constant $C_{s'}$ and $\ell \gg \sigma$ imply that the radiated power is proportional to U^6. The sixth-power formula of Phillips (1956), based on sound measurements of Holle (1938) and Gerrard (1955) for $360 < \mathrm{Re} < 4 \times 10^4$, suggests $C_{s'} \approx 0.11$, assuming $\mathrm{St} \approx 0.2$ and $\ell \gg \sigma$. The underlying sound pressure data however, show a considerable scatter, of the order $\pm 30\%$ (Keefe, 1961). In Leehey and Hanson (1971) mutually connected measurements of sectional r.m.s. lift, spanwise correlation length, Strouhal number, and radiated sound intensity are reported over a Reynolds number range from 4000 to 6450. Within this limited range of Re the associated $C_{s'}$ (based on $C_{L'}$, St and Λ/d) increases from about 0.03 to 0.20. It should be noted, however, that the wire used in Leehey and Hanson is slightly vibrating, the maximum vibration amplitude of about 3% of the diameter occurring at the upper end of the Reynolds number range.

In Fig. 4, the variation of $C_{s'}$ based on present "lift"-data, i.e., $C_{L'}$, St and Λ/d, is shown together with experimental sound pressure data ("sound"-data) of Keefe (1961), Leehey and Hanson (1971) and Iida et al. (1997) (assuming $\ell \gg \sigma$) and the averaged "lift"-data on $C_{s'}$ of Leehey and Hanson (1971). Present formulas suggest that $C_{s'}$ has maximum of about 0.55 at $\mathrm{Re} = 0.3 \times 10^3$, decreases to a broad minimum ($C_{s'} \approx 0.03$) at around $\mathrm{Re} = 2 \times 10^3$ and is approximately constant, $C_{s'} \approx 0.18$, for Reynolds numbers 6×10^3–10^5, in fair agreement with Iida et al. (1997). The data of Leehey and Hanson supports the rapid increase in $C_{s'}$ at around $\mathrm{Re} = 5 \times 10^3$, their sound pressure measurements also show significant deviations from a sixth-power law (Phillips, 1956), as also noted in Etkin et al. (1956). Naturally, deviations from a sixth-power law will occur when $C_{s'}$ varies with Re. In addition, at least for limited aspect ratios ℓ/d, there may be an influence from the variation of σ/ℓ with Re.

3. Review of measurement methods

Various measurement methods for obtaining lift fluctuations are reviewed. Parameters from specific investigations ($\mathrm{Re} < 3 \times 10^5$, $\mathrm{Tu} < 2\%$) are summarized in Table 1.

3.1. Force methods

Methods based on measurement of forces are briefly described; abbreviations F1–F3 refer to the classification in Table 1.

3.1.1. Force element method (F1)

The most direct way of measuring fluctuating lift is to employ a force-sensitive axial segment. In most cases, e.g. Keefe (1961), Moeller (1982) and Bouak and Lemay (1998), the "active" load-transmitting part of the cylinder (of length ℓ_c, see Table 1) is connected to a cantilever beam element that is fixed to a base outside the cylinder or to a base inside one of the "dummy" parts of the cylinder. The force transducer is usually in the form of a strain-gauge arrangement (e.g. Keefe, 1961) but also piezo-elements (e.g. So and Savkar, 1981) and a capacitive voltage divider (Moeller, 1982) have been used. For the design of the cantilever beam/beam springs a compromise between high sensitivity and high natural frequency has to be sought. To minimize effects of vibration the natural frequency is normally designed to be at least four to five times higher than the mean shedding frequency (So and Savkar, 1981). In addition, the deflection and non-resonant oscillation amplitudes of the active part should be kept very small, which requires a high bending stiffness (Fung, 1960). Correction of vibration effects are described in Moeller (1982) and Blackburn and Melbourne (1997).

The complications of having unsealed gaps in between the active cylinder and the dummy parts are first recognized in Keefe (1961). The gaps investigated by Keefe are from 0.4% to 1.8% of the cylinder diameter (d) and unless these gaps are sealed the fluctuating forces are drastically reduced, to a level where $C_{L'}$ is about 10 times lower than with sealing. Apparently, unsealed gaps are used in the towing tank study of Tanida et al. (1973), the gap clearance being approx. 0.7% of d. Unphysically low lift fluctuations without sealing are later confirmed in Kacker et al. (1974) and Moeller (1982). It should be noted that sealing influences the sensitivity of the transducer, statically from the increase in stiffness and dynamically at high frequencies from the added viscous damping of the sealing material (Keefe, 1961). The sealing may also transmit vibration effects and increase the sensitivity to changes in temperature (Moeller, 1982). Interestingly, no sealing is used in the investigation by Bouak and Lemay (1998) but considering the flow development they show convincingly a negligible influence of the gaps, which in their case are only 0.24% of d. The reported r.m.s. lift coefficients by Bouak and Lemay using $\ell_c/d = 1.0$ (same as Keefe), are in excellent agreement with the final results of Keefe (1962), see Fig. 2.

As pointed out already in the pioneering work of Macovsky (1958) there is a reduction in the fluctuating lift coefficient when using a segment of finite length. The r.m.s. lift on a segment of length ℓ_c can be adjusted to sectional r.m.s. lift by using Eq. (4), but this provides knowledge of the lift correlation coefficient function $R_{LL}(s)$, for $s \in [0, \ell_c]$.

3.1.2. Total force method (F2)

In a continuous flow situation, the first quantitative results on fluctuating lift acting on the full cylinder length are reported in Fujino et al. (1958). In most cases using this method the forces on the cylinder are transmitted to one or two transducers that are mounted outside the flow and fixed to a rigid foundation, e.g., see Humphreys (1960) and Sonneville (1976). A complication with the method is that there is always a certain amount of flow distortion towards the cylinder ends (Gerich, 1987), these distortions affects the shedding process which alters the sectional lift distribution (Keefe, 1961; Szepessy and Bearman, 1992). It can be noted that most investigations employing this method have rather limited aspect ratios ℓ/d and do not use controlled end conditions such as end plates (Table 1), a procedure that nowadays is recommended (Stansby, 1974; Fox and West, 1990; Norberg, 1994). End effects are of course subsidiary if the aspect ratio is sufficiently large, under such conditions the total r.m.s. lift is proportional to $\sqrt{\Lambda(\ell - \sigma)}$, assuming partially correlated flow. The conversion to sectional r.m.s. lift is straightforward with known values for Λ and σ, otherwise the total r.m.s. lift or its associated r.m.s. lift coefficient cannot be compared directly with sectional counterparts (or vice versa). Conversions between total and sectional r.m.s. lift are presented in Loiseau and Szechenyi (1972), Sonneville (1976) and West and Apelt (1997).

3.1.3. Electromagnetic method (F3)

This electromagnetic method of estimate sectional r.m.s. lift has so far only been used by Leehey and Hanson (1971). However, the results using this indirect method are fully comparable with other sectional lift methods, e.g., the force-element method (F1) with small ℓ_c/d, see Fig. 2. The method is based on a direct comparison between calculated fluctuating lift causing tiny resonant vibration amplitudes of a taut wire exposed to a uniform flowing air and the electromagnetic force required to excite the same wire to the same amplitude and frequency in still air. The method requires a sufficiently small damping at resonance and that higher harmonics and broad-banded components of the excitation can be neglected.

3.1.4. Momentum method

In Noca et al. (1997) a method of measuring forces from a knowledge of the velocity field (and its derivatives) in a finite and arbitrarily chosen region enclosing an flow-immersed body is presented; see also Unal et al. (1997) and Noca et al. (1999). The method is suited in particular to results from Digital Particle Image Velocimetry (DPIV), for which time sequences of two-dimensional slices of the velocity field can be obtained but not the pressure field, the pressure being the quantity that has been cleverly eliminated by the authors from the original control-volume formulation of the momentum equation.

In Noca et al. (1997) the method is used for calculating fluctuating lift on a stationary circular cylinder for $\mathrm{Re} = 19 \times 10^3$, with the underlying velocity field taken at mid-span using DPIV, in a water tunnel. The method is tested against the total force method (F2), using a force balance ($\ell/d \approx 4.5$). However, the comparison can only be qualitative since method F2 gives out the spanwise-averaged lift and the lift from the momentum method is based on the velocity field at mid-span, using a two-dimensional formulation. Moreover, the calculated lift cannot be exactly the sectional lift since the flow is fully 3-D at this Reynolds number. It is not clear how much the discarded terms due to the missing spanwise velocity component contributes to the calculated lift.

The method appears promising, especially for low-Reynolds number flows where often traditional methods cannot be applied for practical reasons. However, in flows with intrinsic three-dimensional ingredients of relevance for fluctuating lift, given the difficulties in measuring velocity fields other than in single 2-D slices, it may be a fundamental problem for the method's applicability concerning the true sectional lift or the lift on a finite segment length of the cylinder. More comparison tests and validation experiments are needed.

3.2. Pressure methods

Measurement methods based on fluctuating wall pressures are briefly described; abbreviations P1–P7 refer to the classification in Table 1.

Pressure methods rely on the assumption that wall friction have a negligible contribution to the fluctuating lift. Two-dimensional simulations, e.g. Posdziech and Grundmann (2000), suggest that the ratio between pressure r.m.s. lift and total r.m.s. lift varies approximately as $r = 1 - 1.2/\sqrt{\mathrm{Re}}$, the ratio being 0.92 at $\mathrm{Re} = 200$.

Pressure methods do not, as force methods, rely on tiny vibrations of parts or of the full length of the cylinder. Since the cylinder surface is curved, a standard technique for all pressure methods is to employ pressure transducers in a pinhole arrangement (Norberg, 1986), for which the Helmholtz resonance associated with the transducer/pipe cavity puts a limit to the frequency response (Batham, 1973).

3.2.1. Ring of pressure taps (P1)

This method is based on the simultaneous measurement of time-dependent wall pressures at multiple positions around the circumference of the cylinder. Neglecting wall friction, the instantaneous sectional lift coefficient is

$$C_L(t) = \frac{1}{2}\int_0^{2\pi} C_p(\varphi, t)\sin\varphi \,\mathrm{d}\varphi, \tag{17}$$

where $C_p(\varphi, t)$ is the instantaneous pressure coefficient at an angle φ from the stagnation line. All investigations employing this method utilize distributed pressure taps to obtain wall pressures, and by using pressure transducers and summing amplifiers the integral can then be approximated as a sum of weighted terms with an output signal directly monitoring the lift (e.g., Schmidt, 1965) or simply, as in the case of Drescher (1956), the lift can extracted from instantaneous pressure distributions around the circumference. In the pioneering study of Drescher (1956) a total of 12 pressure taps are equally distributed around the cylinder circumference. In subsequent studies, the number of pressure taps varies from 12 (e.g., Mohr, 1981) to 24 (Tunstall, 1970). In some cases, e.g. van Nunen et al. (1972), the pressure taps are distributed in an optimized fashion for approximation of the summed output lift signal. It is mentioned in West and Apelt (1997) that tests had demonstrated the possibility of using only 10 distributed taps/transducers.

3.2.2. Segmented pneumatic averages (P2)

The technique of using manifolds to average pressures from a number of wall tappings was first proposed and used by Surry and Stathopoulos (1977/78). For obtaining the instantaneous sectional pressure lift force, two opposing half-cylinder segments should have wall pressure taps spaced equally across a diametrical line aligned with the oncoming flow and with pressure taps from each segment connected through short tubing to a manifold. The two spatially averaged pressures can be connected either directly to either side of a single differential pressure transducer diaphragm (Gartshore, 1984) or each manifold output can be connected to a pressure transducer, the pressure lift signal then being obtained as the difference between these two pressure outputs (Szepessy and Bearman, 1993). An instantaneous

sectional pressure drag signal can be obtained by rotating the cylinder 90°. Internal flow between tappings on each segment is a source of potential error. Also, for fast response the tubing between pressure taps and the pressure transducer has to be short with a small internal cavity volume in the manifold. The r.m.s. lift coefficients using this technique (Gartshore, 1984; Szepessy and Bearman, 1992) show good agreement with investigations using short force elements (Keefe, 1962) and a full ring of pressure taps (West and Apelt, 1993); see also Fig. 2 and Apelt and West (1996).

3.2.3. Cross-correlation method (P3)

This method relies on the simultaneous measurement of fluctuating wall pressures at two arbitrary and variable positions around the circumference of the cylinder. By using the definition of instantaneous sectional lift, Eq. (17), the sectional r.m.s. lift coefficient can be obtained from (Surry, 1969)

$$C_{L'} = \frac{1}{2}\left[\int_0^{2\pi} \int_0^{2\pi} R_{pp}(\varphi_1, \varphi_2)\, C_{p'}(\varphi_1)\, C_{p'}(\varphi_2) \sin\varphi_1 \sin\varphi_2 \, \mathrm{d}\varphi_1 \, \mathrm{d}\varphi_2 \right]^{1/2}, \tag{18}$$

where $R_{pp}(\varphi_1, \varphi_2)$ is the auto-correlation coefficient, at zero spanwise separation, between wall pressures at circumferential angles (φ_1, φ_2); $C_{p'}$ is the r.m.s. pressure coefficient, $C_{p'} = p'/(\rho U^2/2)$, where p' is the r.m.s. of wall pressure fluctuations. In practice, the two-point measurements can be taken in a way that minimizes the number of unique angle pairs for a certain angular increment ($\Delta\varphi$). Assuming symmetry, the minimum number of such pairs is $N^2 + N + 1$, where $N = \pi/\Delta\varphi$ (Surry, 1969).

For realization of arbitrary angle pairs, the cylinder has to be manufactured in two parts which can be individually rotated. From the practical side, this means that the two pressure taps cannot be located exactly at the same cross-section.

3.2.4. Distribution of r.m.s. pressures, one transducer (P4)

This method, which is approximate but conservative, relies on the assumption that the lift-related pressure fluctuations on the upper and lower side of the cylinder ($\varphi > 0$ and < 0) are completely out-of-phase. If it is further assumed that these pressure fluctuations are dominated by fluctuation energy at around the mean shedding frequency, the following should be a reasonable approximation for the sectional r.m.s. lift coefficient (McGregor and Etkin, 1958):

$$C_{L'} \approx \int_0^{\pi} C_{p'}(\varphi; f_S) \sin\varphi \, \mathrm{d}\varphi, \tag{19}$$

where $C_{p'}(\varphi; f_S)$ is the r.m.s. pressure coefficient, within a frequency band around the mean shedding frequency f_S, at angle φ.

As evident from Eq. (19) the fluctuation energy that really contributes to the fluctuating lift stems from the most upper and lower parts of the cylinder, a region where also the total pressure fluctuation energy is concentrated (Gerrard, 1961; Norberg, 1986). The band-pass filtered r.m.s. pressure coefficient in Eq. (19) then can be replaced by the total r.m.s. pressure coefficient. This resulting $C_{L'}$ can be regarded as an upper bound for the sectional (pressure) lift coefficient, i.e.,

$$\hat{C}_{L'} = \int_0^{\pi} C_{p'}(\varphi) \sin\varphi \, \mathrm{d}\varphi \geqslant C_{L'}. \tag{20}$$

Eq. (19) was originally introduced and employed by McGregor (1957), the slight modification in Eq. (20) is due to Gerrard (1961).

3.2.5. Fluctuating pressures at $\varphi = \pm 90°$ (P5)

The following approximation is provided and used in Kiya et al. (1982):

$$C_{L'} \approx \sqrt{2(1 - R_{pp})}\, C_{p',\,90°}, \tag{21}$$

where $R_{pp} = R_{pp}(90°, -90°)$ is the cross correlation coefficient between wall pressure fluctuations at opposing shoulder positions of the cylinder and $C_{p',\,90°} = C_{p'}(\pm 90°)$. The underlying assumption for Eq. (21) is that the fluctuating lift is dependent primarily on the pressure fluctuations in the vicinity of $\varphi = \pm 90°$ (McGregor, 1957; Bruun and Davies, 1975). Eq. (21) is recovered directly if the instantaneous pressure difference between angles $\pm 90°$ times the cylinder diameter is treated as a direct measure of the sectional lift. The major advantage compared to the full cross-correlation method is that the two pressure taps can be mounted permanently (opposing each other) without any need for a rotation of individual cylinder sections. However, based on the full comparison with other pressure methods, it appears that the formula gives out an overestimation of the true r.m.s. (pressure) lift coefficient (Section 5.1).

3.2.6. Fluctuating pressures at opposing angles $\pm\varphi$ (P6)

This method of estimating the sectional r.m.s. lift coefficient relies on the simultaneous measurement of fluctuating pressures at the opposing angles $\pm\varphi$. Phase, coherence and amplitude information for fluctuating pressures at opposing angles and within a limited number of frequency bands are summed up to give out the sectional r.m.s. lift. The same methodology can be used for the sectional r.m.s. drag and some results on both r.m.s. lift and drag are provided in Norberg (1986). The method was originally developed as a quicker alternative to the time-consuming method P2, the cross-correlation method. The number of angle pairs that has to be tested is only $2N-1$, where again, $N=\pi/\Delta\varphi$.

3.2.7. Distribution of r.m.s. pressures, two transducers (P7)

As validated in Ribeiro (1991) the sectional r.m.s. lift coefficient can be approximated from

$$C_{L'}=\frac{1}{2}(1-R_{BS})\hat{C}_{L'}. \tag{22}$$

R_{BS} is the correlation coefficient of pressure forces acting on both sides of the cylinder (with respect to the wake center line). The factor in front of the upper bound value [$\hat{C}_{L'}$, Eq. (19)] takes into account the lack of a perfect anti-correlation between the upper and lower side. As motivated in Ribeiro (1992) and validated down to about $\mathrm{Re}=2\times10^4$, R_{BS} can be estimated as the correlation coefficient between the shoulders of the cylinder, i.e., $R_{BS}=R_{pp}$ (Fig. 7). Further validation, down to about $\mathrm{Re}=2.7\times10^3$, can be found when comparing present results with previous results using the force element method (F1), e.g. those of Keefe (1962) and Moeller (1982), see Fig. 2.

4. Experimental details

All measurements were carried out in the low-turbulence wind tunnel L2 at department of Thermo- and Fluid Dynamics, Chalmers University of Technology, Gothenburg. The free-stream turbulence intensity is less than 0.06%, while the acoustic noise level is less than 0.6% of the dynamic pressure (Norberg, 1994). The cylinders were mounted horizontally between vertical supporting plates, positioned approximately at the center of the 2.9 m long working section (height $H=1.25$ m, width 1.80 m).

Corrections for solid blockage, using the correction scheme of Maskell (1963), with extension to r.m.s. lift due to Vickery (1966); see also Sohankar et al. (2000), were only applied for blockage parameters $\beta>1.5\%$ ($d\geqslant10$ mm), see Table 2. Corrections for r.m.s. lift were of the same magnitude as the blockage parameter. To match overlapping results for the $d=40$ mm cylinder the level of R_{pp} for the $d=120$ mm cylinder (Fig. 7) was adjusted downwards with a dividing factor of 1.13. This mismatch for R_{pp} is believed to be due mostly to the limited aspect ratio for the largest diameter, $\ell/d=8.8$ (Table 2). As implied from studies on the effects of aspect ratio by Fox and West (1990) and Szepessy (1993), at these Reynolds numbers ($\mathrm{Re}\sim8\times10^4$), a reduction in aspect ratio from sufficiently large values will, eventually, at around an aspect ratio of 10–15, increase the sectional r.m.s. lift. It is suggested that such an increase in fluctuating lift is mostly due to an increase in anti-correlation between the upper and lower sides of the cylinder.

The 3 mm ($d=3.00\pm0.005$ mm) cylinder was a smoothly machined steel rod. For this diameter, only velocity correlation results are provided (Section 5.3). The miniature hot wires were oriented parallel to the cylinder axis. One hot-wire probe could, along the cylinder axis, be traversed sideways in relation to the other (to an accuracy of 0.05 mm and up to a maximum separation of 100 mm) while both probes in conjunction could be moved in all directions

Table 2
Parameters for cylinders of different diameter (d)

d(mm)	3	4	6	10	40	120
ℓ/d	256	105	80	48	26	8.8
d_{EP}/d	10	10	[a]	[a]	[b]	[b]
d/H	0.2%	0.3%	0.5%	0.8%	3.2%	9.6%
β	1.3%	1.3%	1.4%	1.6%	3.7%	11%
s/d	–	0.23	–	–	0.10	0.10
d_h/d	–	5%	–	4%	2%	0.5%

Cylinder length, ℓ; end plate diameter, d_{EP}; working section height, H; solid blockage, β; spanwise distance between pressure taps, s; pressure hole diameter, d_h.

[a] Supporting plates (streamwise length 160 mm) acted as end plates.

[b] End plates of "Stansby design" (Stansby, 1974).

(accuracy approx. 0.1 mm). To within ± 0.2 mm in the streamwise direction and to within ± 0.1 mm crosswise the two hot wires were positioned at the same relative position in a cross-sectional plane. A similar experimental setup was used for the correlation measurements with the 6 mm cylinder, see Norberg (1987a).

The 4 mm ($d = 3.98 \pm 0.01$ mm) cylinder contained two small-scale pressure transducers (outer diameter 2.3 mm) that were mounted opposing each other in a one-piece cylindrical section made of aluminum (length 33 mm). The cavities in front of the transducers were connected to the outer surface by drilling two diametrically opposing holes of diameter $d_h = 0.2$ mm at a spanwise distance of $s = 0.9$ mm. By threading of this central section with two 5 mm long extensions on each side an efficient tightening of the pinhole housings was achieved. Finally, the full cylinder length was realized by adding two 240 mm long dummy stainless tubes screwed on to each side of the instrumented section. The cannulas for back-venting the transducers were extended to outside the wind tunnel by hypodermic tubes. The frequency responses could both be described as a second-order system with a natural frequency of $f_n = 4.9$ kHz and a damping factor of $\zeta \simeq 0.15$. The individual systems could be tuned to a flat response (± 1 dB) from DC to about 5 kHz. Based on the maximum amplification (gain = 500) of the two-channel bridge amplifier the sensitivities were 13.4 and 14.1 mV/Pa, respectively (accuracy $\pm 2\%$). The resulting noise level at 1 Hz to 3 kHz was about 0.1 Pa.

The 10 mm ($d = 10.0$ mm) hollow cylinder contained, at mid-span, a quarter-inch microphone with a sensitivity of (4.1 ± 0.06) mV/Pa. The pinhole arrangement could be described as a second-order system ($f_n = 1.7$ kHz, $\zeta = 0.3$). The resulting noise level was negligible (less than 0.01 Pa). Instrumentation and pinhole system for the 40 mm cylinder ($d = 40.4$ mm) were similar to an earlier investigation (Norberg, 1986). Instrumental details for the 120 mm cylinder can be found in Norberg and Sundén (1987).

The overall uncertainty for r.m.s. pressure coefficients was estimated to be $\pm 2.5\%$ (at constant odds 20:1). The corresponding uncertainty for Reynolds numbers was $\pm 0.5\%$ ($\pm 0.8\%$ at velocities less than 4 m/s).

Based on repeated measurements and error analysis of Bendat and Piersol (1984), the uncertainty in the reported correlation coefficients was estimated to be ± 0.02 (± 0.01 for absolute correlation levels higher than 0.8). The overall uncertainty for r.m.s. lift coefficients, Eq. (22), was $\pm 4\%$. Spanwise correlation lengths had a typical overall uncertainty of about $\pm 5\%$.

5. Results and discussion

5.1. Fluctuating wall pressures and sectional lift

The sectional r.m.s. lift on the cylinder was obtained using pressure method P7 (Section 3.2.7). As a measure for the correlation between sectional lift-related forces on the upper and lower side of the cylinder ($\varphi > 0$ and < 0) the correlation coefficient R_{pp} between fluctuating wall pressures at $\varphi = \pm 90^\circ$ was used, i.e.,

$$C_{L'} = \frac{1}{2}(1 - R_{pp}) \int_0^\pi C_{p'}(\varphi) \sin\varphi \, \mathrm{d}\varphi. \tag{23}$$

R.m.s. pressure distributions $C_{p'}(\varphi)$ at 10 different Re are depicted in Fig. 5; $R_{pp}(\mathrm{Re})$ is shown in Fig. 7. Results for $C_{p'}(90^\circ)$ and $C_{L'}(\mathrm{Re})$ are presented in Figs. 6 and 8. A summary of cases is provided in Table 3.

Distributions of the r.m.s. pressure coefficient around the cylinder surface reflect the sectional fluctuating pressure loading and as is evident from Fig. 5 an exceptional low loading of fluctuating pressure forces is indicated at around $\mathrm{Re} = 1.5 \times 10^3$. Extensive measurements of r.m.s. pressures at $\varphi = 90^\circ$ (Fig. 6) and $\varphi = 180^\circ$ (not shown) revealed that the minimum loading occurred at $\mathrm{Re} = (1.51 - 1.62) \times 10^3$, where also a minimum was reached for the absolute value of R_{pp} (Fig. 7). Consequently, there appears to be a local minimum in the sectional r.m.s. lift coefficient at $\mathrm{Re} \simeq 1.6 \times 10^3$, the indicated minimum level was $C_{L'} \simeq 0.045$ (Table 3). At around this particular Re there is also a local minimum in the mean pressure loading, with a mean pressure drag coefficient of about 0.9 (Norberg, 1993a) and a base suction ($-C_{pb}$) of 0.8 (Norberg, 1994).

Being indicative of the overall low levels of acoustic noise and free-stream turbulence, all distributions in Fig. 5 exhibited a very low level of $C_{p'}$ at the frontal stagnation line ($\varphi = 0^\circ$). The $C_{p'}(0^\circ)$ was about 0.6%, except for the distribution at the lowest velocity for the smallest diameter ($d = 4$ mm, $U = 2.7$ m/s, $\mathrm{Re} = 0.72 \times 10^3$) where transducer noise increased this minimum level to about 1.5%. From this low stagnation value there was a steady increase in $C_{p'}$ up to a local maximum at φ_s (Table 3) associated with flow separation. The maximum in $C_{p'}$ occurred slightly upstream of the point where there is a maximum in the mean pressure gradient (Norberg, 1993a). At $\mathrm{Re} = 0.72 \times 10^3$ the angular distance between these two points was about 2°, whereas at $\mathrm{Re} = 2.1 \times 10^5$ the points were only separated by about 0.5°. Interestingly, the gradual decrease in φ_s with increasing Re was interrupted in between $\mathrm{Re} = 5 \times 10^3$ and 8×10^3. In between $\mathrm{Re} = 7.2 \times 10^3$ and 8.1×10^3 there was instead a slight (about 2°) downstream movement of φ_s, the

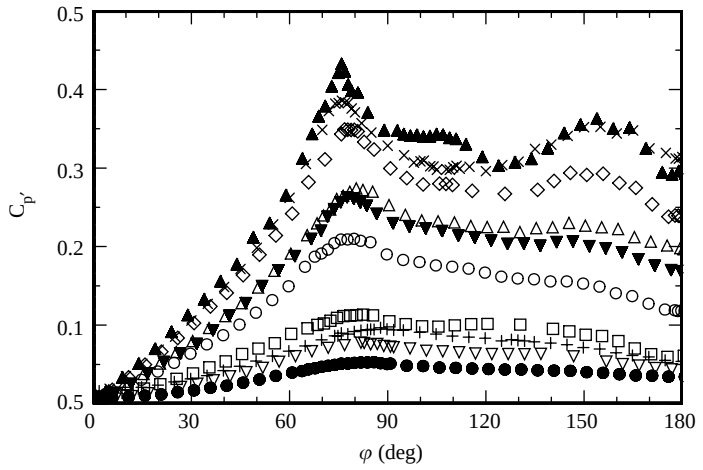

Fig. 5. R.m.s. pressure distributions, $C_{p'}(\varphi)$, for Re: +, 7.2×10^2; ●, 1.5×10^3; ▽, 4.4×10^3; □, 5.0×10^3; ○, 6.1×10^3; ▼, 7.2×10^3; △, 8.1×10^3; ◇, 2.0×10^4; ×, 6.1×10^4; ▲, 2.1×10^5.

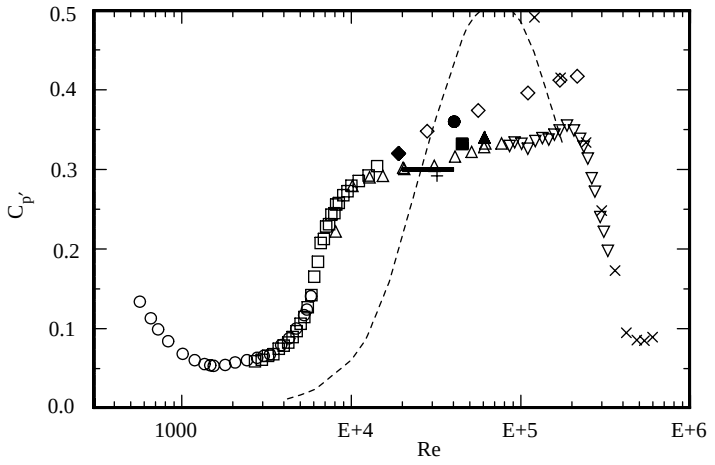

Fig. 6. R.m.s. pressure coefficient at $\varphi = 90^\circ$: broken line, Gerrard (1961); ▩, $\ell/d = 13$, $\beta = 6\%$ (Sonneville, 1973); ×, $\ell/d = 10$, $\beta = 13\%$ (Bruun and Davies, 1975); ◆, $\ell/d = 11$, $\beta = 3\%$ (Novak and Tanaka, 1977); +, $\ell/d = 8$, $\beta = 8\%$ (Norberg, 1986); ▽, $\ell/d = 9$, $\beta = C$ (Norberg and Sundén, 1987); ——, $\ell/d = 7$, $\beta = 0$ (Kiya and Tamura 1989); ◇, $\ell/d = 15$, $\beta = 10\%$ (West and Apelt, 1993); ●, $\ell/d = 20$, $\beta = 6\%$ (Lee and Basu, 1997); present: ○, $\ell/d = 105$, $\beta = 1\%$; □, $\ell/d = 48$, $\beta = C$; △, $\ell/d = 28$, $\beta = C$ ("$\beta = C$" means that results have been corrected for blockage).

indicated mean separation point. At around these Reynolds numbers there is also a build-up of a secondary maximum in $C_{p'}$ at $\varphi \approx 155^\circ$, which for $\mathrm{Re} > 8 \times 10^3$ and all the way up to the drag crisis is a characteristic feature of the r.m.s. pressure distributions (Fig. 5); see also Norberg and Sundén (1987) and West and Apelt (1993). As discussed in Norberg and Sundén (1987) the reason for this secondary maximum to show up is the occurrence of relatively unusual but powerful suction peaks; see also Norberg (1986).

Results for $C_{p'}(90^\circ)$, extending down to $\mathrm{Re} = 0.57 \times 10^3$, are shown in Fig. 6. There is a dramatic variation with Re, the highest value (at $\mathrm{Re} \simeq 2 \times 10^5$) being about 7 times higher than the lowest (at $\mathrm{Re} \simeq 1.6 \times 10^3$). The largest variations occurred between $\mathrm{Re} = 5 \times 10^3$ and 7×10^3 and within this short interval there was a doubling in $C_{p'}(90^\circ)$, from 0.11 to 0.22. In Gerrard (1961) even larger variations of $C_{p'}(90^\circ)$ are presented, see Fig. 6. Presumably, the pressure gauge design in Gerrard (1961) with a very large pressure-sensitive area in combination with spanwise flow inhomogeneities and effects of blockage for high Reynolds numbers are responsible for most of the differences as compared with present

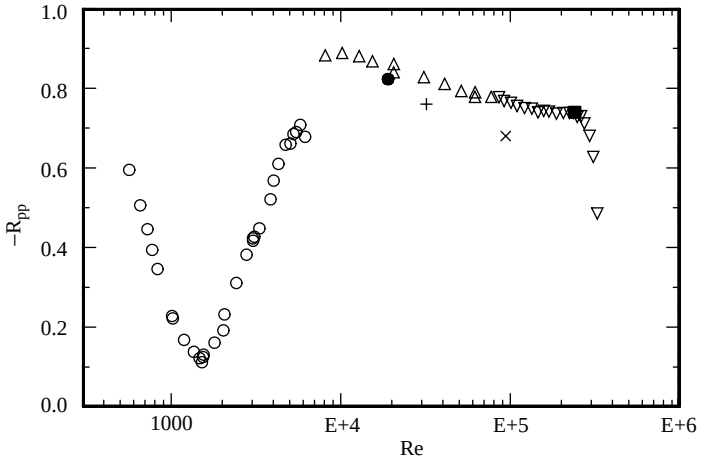

Fig. 7. Correlation coefficient of fluctuating pressures at $\varphi = \pm 90^{\circ}$: ▩, Bruun and Davies (1975); ●, Novak and Tanaka (1977); + Kiya et al. (1982); ×, Taniguchi and Miyakoshi (1990); present: ○, $d = 4$ mm; △, $d = 40$ mm; ▽, $d = 120$ mm.

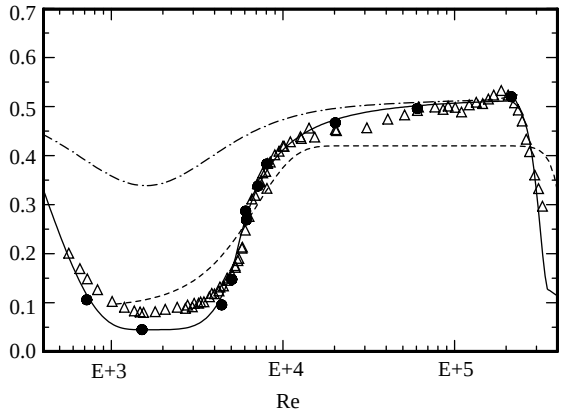

Fig. 8. Sectional r.m.s. lift coefficient versus Re: ●, present; △, approximation $1.5 \times C_{p'}(90^{\circ})$ (present data); dot-broken line, from vortex street model of Chen (1971a,b) using mean pressure drag coefficients and Strouhal numbers from Norberg (1993a, 1994); broken line, formula given by Engineering Science Data Unit (ESDU, 1985); solid line, present formulas (Appendix A).

Table 3
Summary of results from r.m.s. pressure distributions, $C_{p'}(\varphi)$

$\mathrm{Re}/10^4$	d(mm)	St	φ_S (deg)[a]	$C_{p'}(\varphi_s)$	$C_{p'}(90^{\circ})$	$C_{p'}(180^{\circ})$	$\hat{C}_{L'}$	$-R_{pp}$	$C_{L'}$
0.072	4	0.210	88	0.10	0.10	0.05	0.15	0.45	0.11
0.15	4	0.212	85	0.05	0.05	0.03	0.08	0.12	0.045
0.44	4	0.210	82	0.08	0.07	0.04	0.12	0.63	0.10
0.50	10	0.209	81	0.11	0.10	0.06	0.18	0.68	0.15
0.61	10	0.207	79	0.21	0.19	0.12	0.31	0.73	0.27
0.72	10	0.204	78	0.26	0.23	0.17	0.38	0.77	0.34
0.81	10	0.203	80	0.27	0.25	0.20	0.41	0.88	0.38
2.03	40	0.194	78	0.35	0.30	0.24	0.50	0.86	0.47
6.10	40	0.187	77	0.38	0.33	0.31	0.56	0.78	0.50
21.4	120	0.189	76	0.43	0.35	0.30	0.60	0.74	0.52

[a] φ_s is angle for maximum $C_{p'}$.

and other results (Fig. 6). When considering the differences in blockage, aspect ratio, end conditions and level of free-stream turbulence there is, except for Gerrard (1961), a reasonable agreement between present and previous results. For instance, the results of West and Apelt (1993) in Fig. 6 are taken with a blockage parameter of $\beta = 9.5\%$, a free-stream turbulence intensity level of $Tu = 0.2\%$ and an aspect ratio of $\ell/d = 15$ using end plates. Here it can be inferred that the combination of higher blockage (Vickery, 1966; Richter and Naudascher, 1976) and free stream turbulence (Norberg, 1987a) is the cause for the slightly higher levels. Note that the present results have been corrected for blockage effects, but only for $\beta > 1.5\%$.

In Fig. 2 it should be mentioned that also the results of Mohr (1981) have been corrected for blockage effects (by the author). Due to lack of mutually connected results of r.m.s. lift, mean pressure drag and base suction, other experimental results in Fig. 2 are left uncorrected for blockage ($\beta \leqslant 10\%$, see Table 1). Experimental data included in Fig. 2 has been considered reliable in terms of a sufficiently large cylinder aspect ratio (ℓ/d) in combination with suitable end conditions (Norberg, 1994). The rather high $C_{L'}$-levels of Moeller and Leehey (1984) for $Re \geqslant 10^4$ (Fig. 2) are not believed to be due to effects of blockage nor aspect ratio ($\beta = 3.1\%$, $\ell/d = 26$). Here the main reason for the elevated levels is due probably to effects of free-stream turbulence intensity, which in their case (water measurements) is $Tu = 0.9\%$. As shown in Norberg and Sundén (1987), for $10^4 < Re < 10^5$, an increase in turbulence intensity from 0.1% to 1.4% gives an approximate 15% increase in the sectional r.m.s. lift. For $Re \geqslant 10^4$, the $C_{L'}$-results of Keefe (1962), see Fig. 2, are slightly lower than the present. Here the main reason is believed to be the finite spanwise extent of the force element ($\ell_c/d = 1$), which in relation to the spanwise correlation length, at these Re, show a decrease with increasing Re, see Fig. 3. As outlined in Section 2.1, also see West and Apelt (1997), the reduction in $C_{L'}$ due to this averaging effect can be corrected. If doing this, using the proposed function Λ/d versus Re (Appendix A), there is actually a very good agreement with the present data. However, in this study, all results for r.m.s. lift are left uncorrected for this effect.

As seen in Fig. 8, especially for $Re > 5 \times 10^3$, the sectional r.m.s. lift coefficient can be roughly approximated as $C_{L'} \approx 1.5 \times C_{p'}(90^\circ)$. From this interrelation it can be inferred that for the present turbulence intensity of $Tu = 0.06\%$ the rapid drop in $C_{L'}$ when entering the critical regime occurred at $Re \simeq 2.3 \times 10^5$. As seen in Fig. 5 the $C_{p'}$-distribution for $Re = 2.1 \times 10^5$ exhibits a peak behavior at around $\varphi = 105^\circ$. This peak is associated with transition to turbulence in the separated shear layers, which at these Re occurs very soon after separation (Smith et al., 1972). As evident, the subsequent development of flow reattachment results in a rapid fall in $C_{L'}$ (Norberg and Sundén, 1987).

The $C_{L'}$-formula suggested by Kiya et al. (1982), Eq. (21), as used also in Norberg and Sundén (1987), does not fit very well with existing experimental sectional data (Fig. 2). For $Re > 5 \times 10^3$, the ratio between r.m.s. lift calculated from the formula given by Kiya et al. (1982) and Eq. (23) is 1.28 ± 0.04. This implies that the lift coefficients presented by Norberg and Sundén (1987) are largely overestimated. If, however, the coefficients in Norberg and Sundén (1987) are reduced by a factor 1.28, a much better agreement with present results is found.

For $6 \times 10^3 < Re < 3 \times 10^5$, the formula for $C_{L'}$ given by ESDU (1985) ($Re \geqslant 10^3$, see Fig. 8) appears to underestimate the sectional r.m.s. lift, also see Fig. 2, whereas at lower Re, based on the results of Keefe (1962), Leehey and Hanson (1971), Moeller and Leehey (1984) and the present results, the opposite seems likely. Interestingly, the value of $C_{L'} \simeq 0.1$ at $Re = 10^3$ as indicated from ESDU (1985) appears not to have been based on the above mentioned two studies prior to 1985, but rather on the results of Tanida et al. (1973), presumably with some guidance towards lower Re from the results of Keefe (1962) and Bishop and Hassan (1964). However, the results of Tanida et al. (1973) cannot be regarded as fully reliable since they have, in their towing tank experiments, an aspect ratio of only about 10 (one end is penetrating the liquid surface, the other is close to the bottom of the tank, no end plates). In particular and due mainly to this limited aspect ratio (Norberg, 1994) their results within the laminar shedding regime ($Re = 60$–110), using oil as the working medium, should be treated with great caution. Apart from the oil data of Tanida et al. (1973), and prior to the results of the author (Norberg, 1993a), the lowest attained Re on fluctuating lift is due to Moeller and Leehey (1984) who for their lowest Re of 2.7×10^3 report $C_{L'} = 0.07$, in agreement with present results, see Fig. 2.

Also shown in Fig. 8 is a curve for $C_{L'}(Re)$ as deduced from the procedure of Chen (1971a, b), based on a far-field control volume analysis of the vortex street. The procedure needs as input only the Strouhal number and the mean pressure drag coefficient, as in this case were taken (as smoothed data) from the author's previous measurements (Norberg, 1993a, 1994). However, the analysis of Chen is two-dimensional to its nature, assumes harmonic lift variations and completely ignores flow developments close to the cylinder. Despite the severe restrictions on the analysis of Chen, the indicated correct level of $C_{L'} \simeq 0.5$ at the end of the subcritical regime ($Re \simeq 2 \times 10^5$) seems to have been captured. However, the indicated very rapid drop in $C_{L'}$ towards $Re \simeq 1.6 \times 10^3$ is not captured. For turbulent shedding conditions, the author does not think that a control volume analysis based on far-field conditions, with empirical input of only mean drag and shedding frequency, will ever fully capture the true velocity variation of fluctuating forces on a bluff body. To be reliable, such a model has to take into account the subtle and strongly multi-dimensional flow variations close to the body, which in fact are responsible for the load fluctuations. In closure and relating to the vortex

street analysis of Chen (1971a, b), the author believes that the close agreement with experiments at $\mathrm{Re} \sim 10^5$ is fortuitous.

5.2. Fluctuating lift and wall pressures at $\varphi = \pm 90^\circ$

The indicated very large variation in fluctuating pressure loading for Reynolds numbers in between 1.6×10^3 and 10^4, in particular at around $\mathrm{Re} = 5 \times 10^3$, needs further elucidation. As pointed out in several previous publications by the author (Norberg, 1987a,b, 1989, 1992, 1993a,b, 1994, 1998), these dramatic variations are believed to be due to a fundamental change in the near-wake shedding process, related to intrinsic three-dimensional effects. Some further signatures of this transitional behavior can be traced from the coupling between fluctuating pressures between opposing angles $\varphi = \pm 90^\circ$.

Shown in Fig. 9 are fluctuating pressures at $\varphi \pm 90^\circ$ (at mid-span) and their instantaneous difference, scaled with corresponding r.m.s.-values ($\mathrm{Re} = 3.1 \times 10^3$ and 20×10^3, respectively). This pressure difference can be seen as a rough estimate of the instantaneous sectional pressure lift. As is evident from Fig. 9, the individual pressure variations at

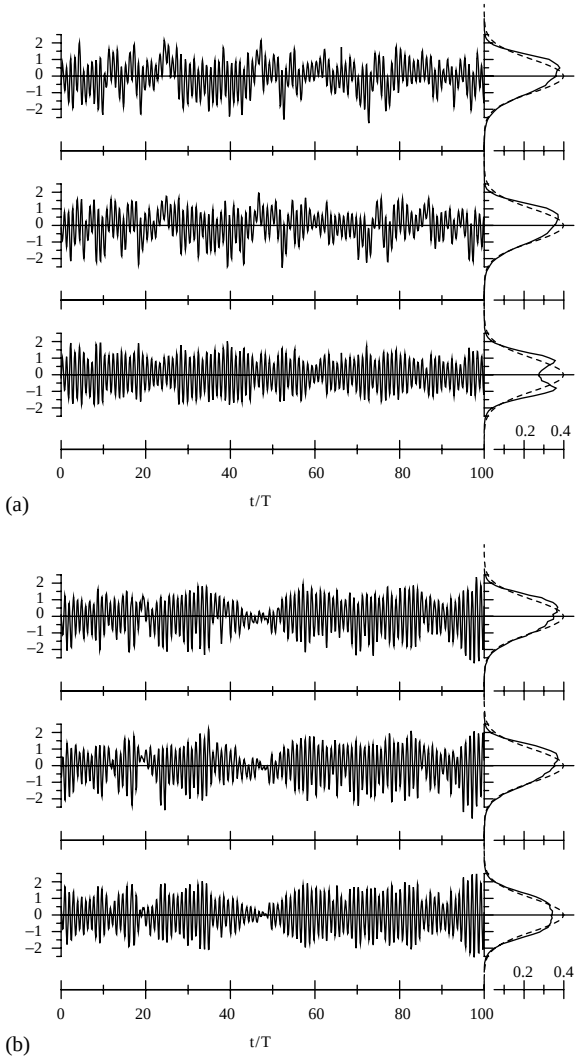

Fig. 9. Fluctuating pressures at $\varphi = \pm 90^\circ$ and their difference mimicing the behavior of sectional lift. (a) $\mathrm{Re} = 3.1 \times 10^3$, $d = 4$ mm, (b) $\mathrm{Re} = 2.0 \times 10^4$, $d = 40$ mm. Upper: $\varphi = +90^\circ$; middle: $\varphi = -90^\circ$; lower: difference $p(90^\circ) - p(-90^\circ)$. Signals are scaled with corresponding r.m.s. values and cover a time interval of 100 mean shedding periods ($T = f_S^{-1}$). Probability density functions are shown on right (dotted: Gaussian).

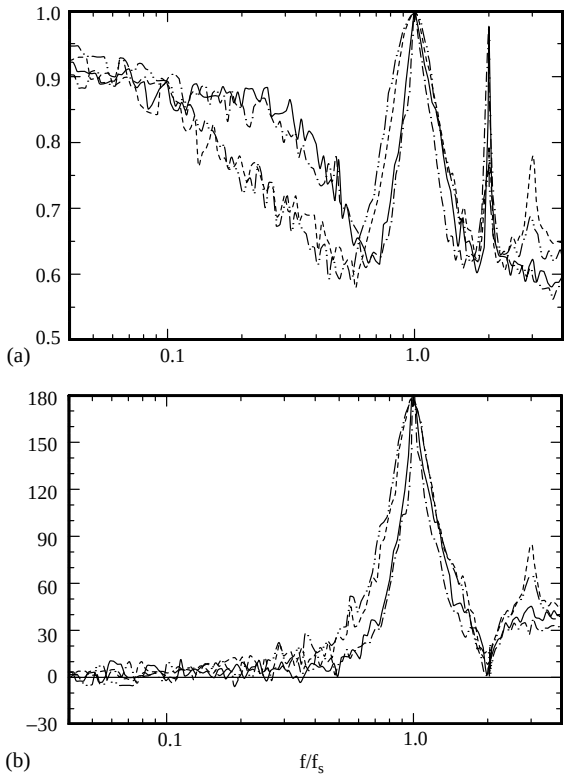

Fig. 10. (a) Coherence function γ^2 and (b) phase Φ (in deg) between fluctuating pressures at $\varphi = \pm 90^\circ$: dot-broken line, Re $= 1.6 \times 10^3$; solid line, Re $= 3.1 \times 10^3$; broken line, Re $= 20 \times 10^3$; double-dot-broken line, Re $= 61 \times 10^3$.

$\varphi = \pm 90^\circ$ display a highly irregular behavior, with negatively skewed probability density functions (shown on right). For both Reynolds numbers the pressure fluctuation energy is dominated by frequencies at and around the mean shedding frequency. However, the pressure signals, for both Re, also have a significant contribution from low frequencies. From Fig. 10 the instantaneous pressure difference (mimicing sectional lift) displays a highly coherent out-of-phase behavior at around the mean shedding frequency (f_S). There is also, for low frequencies, lower than about $0.1 \times f_S$, a high coherence in between these two locations (coherence factor of about 0.9). However, as shown in Fig. 10(b), the phase difference is close to zero which means that these low-frequency components do not contribute to the fluctuating lift (as do not the pressure fluctuation energy at around two times the mean shedding frequency). The appearance of the spectra from the instantaneous pressure difference (not shown) was in general accordance with true lift spectra as shown, e.g., in Keefe (1961), Sonneville (1976) and Moeller (1982) (Re $\sim 5 \times 10^4$). One notable difference, however, was the significant sharpening of the shedding peak (centered around f_S) when coming to Reynolds numbers less than about 5×10^3, in agreement with previous findings by the author, e.g., Norberg (1993a). The same effect can be traced also from the coherence and phase functions, see Fig. 10.

There was a much higher regularity in the envelop amplitude of indicated fluctuating lift at low Reynolds numbers, lower than about Re $= 6 \times 10^3$, as compared with higher Re. As seen in Fig. 9, the lift-related signal for Re $= 3.1 \times 10^3$ has a fairly regular amplitude variation with no apparent excursions down to very low levels, close to zero, as was found as a typical event only at higher Re, see Fig. 9(b). This is also evidenced from the change in appearance of the (symmetrical) probability density function (PDF) of the lift-related signals (Fig. 9). For Re $< 6 \times 10^3$, approximately, the lift-related PDFs were similar to those of a sine wave with random noise (two peaks) whereas for higher Re the PDFs were more like that of a narrow band, random noise function (one peak), see Bendat and Piersol (1984). In Fig. 9(b), for Re $= 20 \times 10^3$, such an event of very low amplitude is depicted (at around $t/T = 47$). These events are believed to be due to near-cylinder vortex dislocations causing intermittent major disturbances to the evolvement of vortex shedding (Norberg, 1993a). They appear to be a characteristic feature of turbulent shedding flow, but only for Reynolds numbers higher than about 6×10^3. The duration of these events was of the order 10 shedding periods.

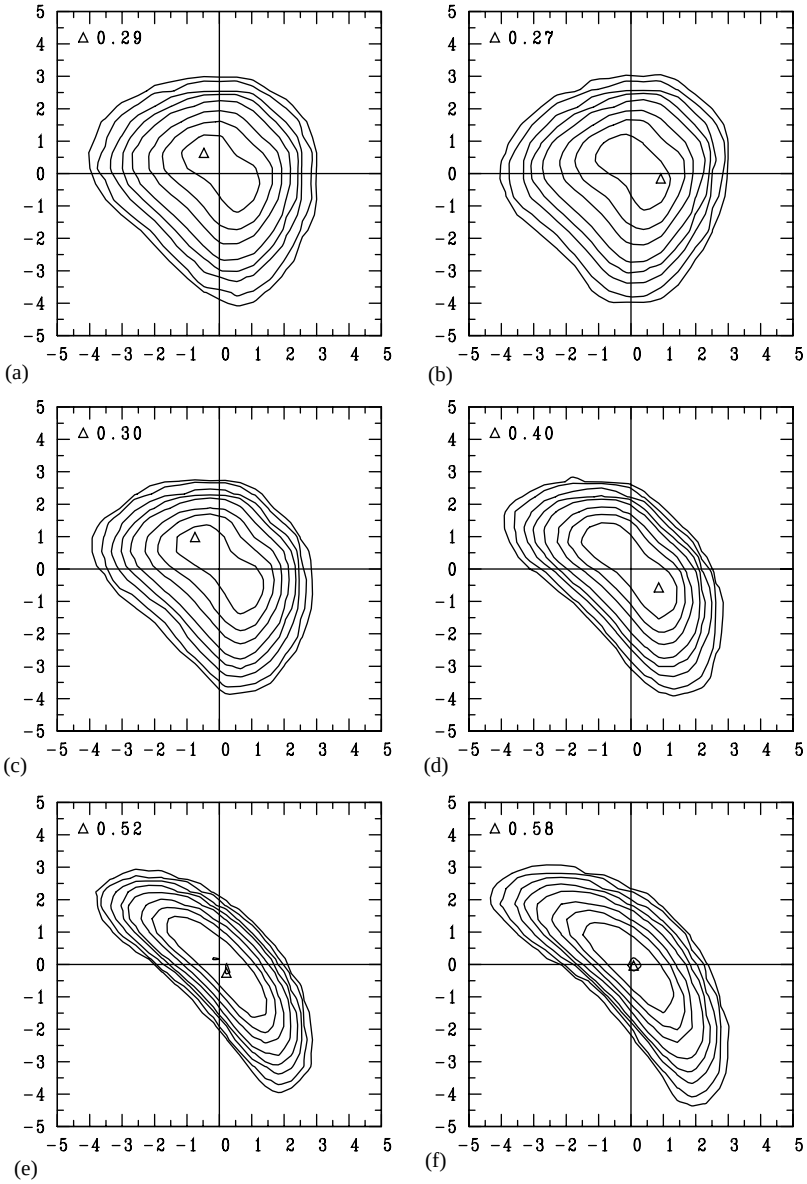

Fig. 11. Joint probability density functions between fluctuating pressures at $\varphi = \pm 90^\circ$. (a) $\mathrm{Re} = 1.0 \times 10^3$ ($d = 4$ mm), (b) $\mathrm{Re} = 1.5 \times 10^3$ ($d = 4$ mm), (c) $\mathrm{Re} = 3.1 \times 10^3$ ($d = 4$ mm), (d) $\mathrm{Re} = 5.1 \times 10^3$ ($d = 4$ mm), (e) $\mathrm{Re} = 2.0 \times 10^4$ ($d = 40$ mm), (f) $\mathrm{Re} = 6.1 \times 10^4$ ($d = 40$ mm). Scaling with local r.m.s. values. Iso-levels: 0.001, 0.002, 0.005, 0.01, 0.02, 0.05, 0.1, 0.2 and 0.5. Triangles indicate maximum levels.

However, no characteristic time interval in between such events was found. They appeared to to be completely random in time. For high Reynolds numbers and when following the amplitude and frequency in time, utilizing the Hilbert transform (Bendat and Piersol, 1984), it was found that high lift-related amplitudes in general were coupled to shedding frequencies lower than the mean value. For lower Re, lower than about 6×10^3, there was no such apparent coupling; see also Norberg (1989). Conceivably, it takes longer time to generate the lift-related von Kármán vortices within periods of strong vortex shedding.

Further characteristic differences between results for low and high Re, related to pressure loading signatures and fluctuating lift, can be seen in Fig. 11, displaying iso-contours of the joint probability function (JPDF) between pressures at $\varphi = \pm 90^\circ$ ($\mathrm{Re}/10^3 = 1$–61).

A straight line at an angle -45° from the horizontal would mean two signals which are perfectly anti-correlated, whereas two completely random and independent functions would produce a circular distribution with its highest peak at the origin (Bendat and Piersol, 1984). In rough terms, the two last distributions, $\mathrm{Re} = 20 \times 10^3$ (Fig. 9(e)) and $\mathrm{Re} = 61 \times 10^3$ (Fig. 9(f)), can be characterized as a mixture of the two above model functions. However, for low levels of the JPDF the distributions are cusped, away from the diagonal of perfect anti-correlation. For events creating this cusped signature one signal makes a relatively strong negative excursion while the other has a rather limited positive amplitude. In fact, unusual but powerful events with large suction peaks downstream of separation, in particular at around $\varphi = 155^\circ$ but also sensed at $\varphi = 90^\circ$, were recorded, but only for Reynolds numbers greater than about 6×10^3, see also Norberg (1986) and Norberg and Sundén (1987). The JPDFs at lower Re appear to be more complex, see Fig. 11(a–d). Here the distributions have two peaks along the line of perfect anti-correlation, with a characteristic waist in between. With decreasing Re, the distributions become wider, the maximum JPDF-level decreases and besides the central peak region, which is directed along the anti-correlation line, there is also, at low JPDF-levels, a rather strong directivity bias towards the line for a perfect correlation (pointing 45° upwards). This last effect, as found only for these low Reynolds numbers, is probably related to the relatively strong coherence for the in-phase frequency components at low frequencies, see Fig. 10.

In rough terms, the degree of wideness of the JPDFs is inversely proportional to its peak value (given in each sub-figure). The change in wideness of the JPDFs is also reflected in the rapid change of $-R_{pp}$ that occurs in between $\mathrm{Re} \simeq 2 \times 10^3$ and 8×10^3 (Fig. 7). It is worth noting that $-R_{pp}$ exhibited a maximum at $\mathrm{Re} \simeq 10^4$. However, between $\mathrm{Re} = 10^4$ and 2.6×10^5 there was only a slight drop in $-R_{pp}$, in rough agreement with previous data, see Fig. 7. This drop in anti-correlation is supposed to be due to effects of transition to turbulence in the separated shear layers. As compared with the present data, the slightly lower level of $-R_{pp}$ as found by Taniguchi and Miyakoshi (1990) for $\mathrm{Re} = 9.4 \times 10^4$ is due probably to that no end plates are used ($\ell/d = 14$). At such a limited aspect ratio and without using end plates the shedding flow is expected to be weakened (Moeller, 1982). As a consequence there will be a less coupling in between the opposing shoulder points of the cylinder.

5.3. Spanwise correlations

To obtain the r.m.s. lift on a finite spanwise section of the cylinder the sectional r.m.s. lift has to be complemented with information on the spanwise coupling of sectional and fluctuating lift forces. As outlined in Section 2.1, this information is provided from the correlation function $R_{LL}(s)$ where s is the spanwise separation. In this study, as motivated in Section 2.1, the correlation function R_{LL} was estimated from hot-wire measurements of fluctuating velocities just outside the separated shear layers close to the cylinder, $R_{LL}(s) \approx R_{uu}(s)$. Further motivation for this approximation comes from that turbulence intensity levels in these regions appear to be closely related to the sectional r.m.s. lift coefficient (Gerrard, 1965; Moeller, 1982); see also Unal and Rockwell (1988). This interrelationship was

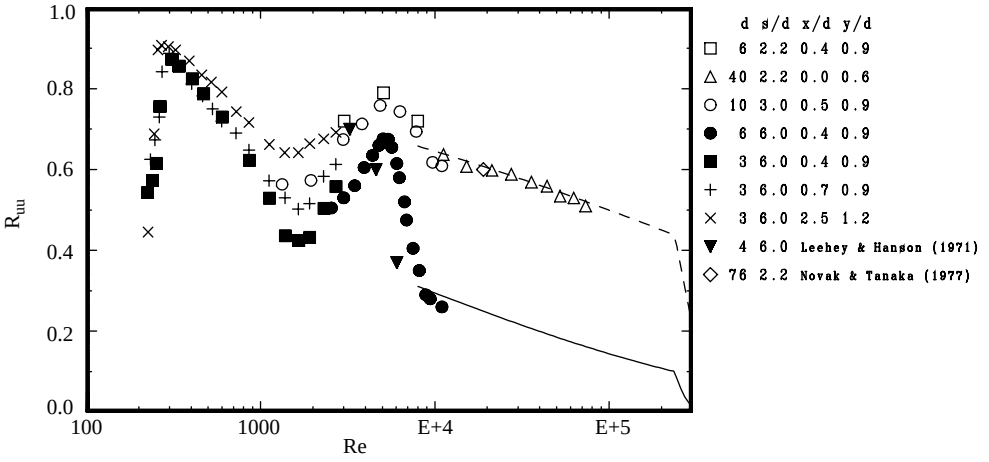

Fig. 12. Spanwise correlation coefficient of fluctuating velocities. Solid and dotted lines represent variations as calculated from formulas for Λ/d (Appendix A) using $\exp(-s/\Lambda)$ as approximation. Cylinder diameter d (in mm), relative spanwise separation s/d, and relative positions in the cross-sectional plane $(x/d, y/d)$ are indicated on right.

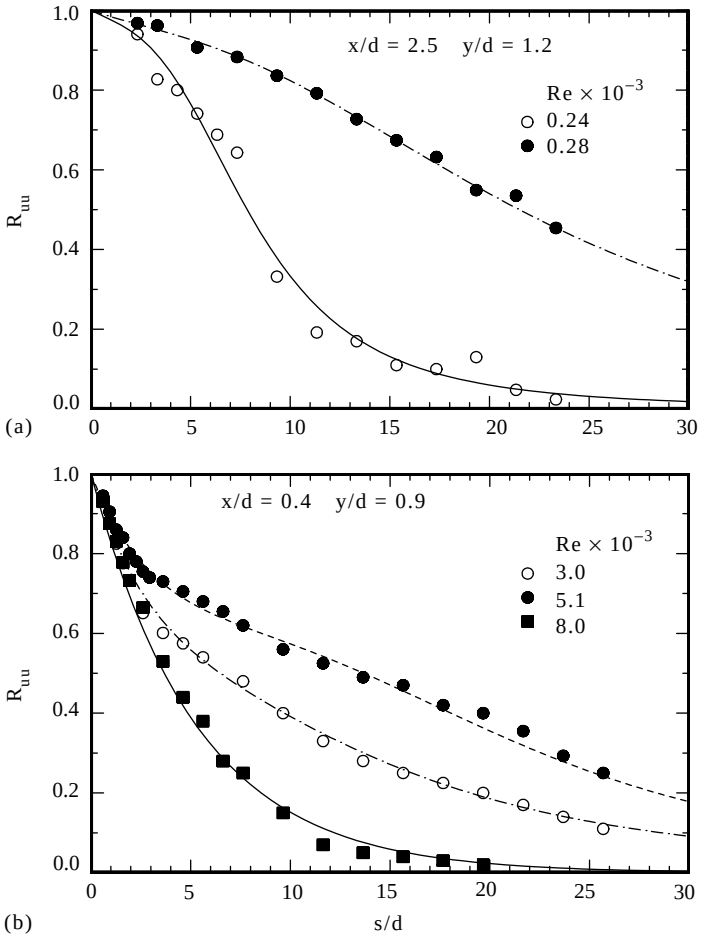

Fig. 13. Correlation coefficient versus relative spanwise separation. (a) $d = 3$ mm. Solid line: $\Lambda_1/d = 4$, $\Lambda_2/d = 10$, $n = 3.0$, $\alpha = 0.90$. Dot-broken line: $\Lambda_1/d = 4$, $\Lambda_2/d = 31$, $n = 2.4$, $\alpha = 0.93$. (b) $d = 6$ mm. Broken line: $\Lambda_1/d = 3$, $\Lambda_2/d = 22$, $n = 2.4$, $\alpha = 0.49$. Dot-broken line: $\Lambda_1/d = 3$, $\Lambda_2/d = 27$, $n = 3.0$, $\alpha = 0.61$. Solid line: $\Lambda_1/d = 5.3$, $\alpha = 0$. Relative positions (x/d, y/d) of hot wires are indicated.

noted also from the present measurements. To within the experimental accuracies the two hot wires were always at the same relative position within a cross-sectional plane. However, the actual position in this plane was found to be of some importance. For most of the results presented here the relative position was $x/d = 0.4$–0.5 and $y/d = 0.9$, with origin at the cylinder axis. The Reynolds number range covered is from about 0.24×10^3 to 75×10^3. Results showing the effects of Re on R_{uu}, at some selected relative spanwise separations s/d, are shown in Fig. 12. Distributions of $R_{uu}(s/d)$ at various Re are shown in Fig. 13. Spanwise correlation lengths are found in Fig. 3.

The perhaps most striking features in Fig. 12 are the two local maxima in R_{uu} as found at Reynolds numbers of about 0.3×10^3 and 5×10^3 (with a local minimum in between, at $\mathrm{Re} \simeq 1.6 \times 10^3$). Apart from these, the general trend with increasing Re is a decrease in spanwise correlation.

As for the second local maximum in spanwise correlation (at $\mathrm{Re} \simeq 5 \times 10^3$) the first measurements showing this behavior was published in Norberg (1987a); see also Norberg (1989). Based on the variation of $R_{uu}(s/d = 6.0)$ with Re (Fig. 12), the peak occurs at $\mathrm{Re} = 5.1 \times 10^3$ ($d = 6$ mm). The author later (Norberg, 1992) carried out some additional measurements with a larger diameter ($d = 10$ mm). Although this later study was not as extensive as the first one it still gave as a result this remarkable peak behavior at around $\mathrm{Re} = 5 \times 10^3$ (Fig. 12, $s/d = 3.0$). It is worth noting that the two cylinders have completely different aeroelastic properties (solid steel rod of diameter 10 mm as compared with a hollow steel tube of outer diameter 6 mm). This seems to rule out the possibility that the resonant-like peak behavior is due to vibrational effects. At around this Re there is also a fundamental change in the spectral quality of the shedding frequency, as proven from extensive experiments by the author with various cylinder diameters and aspect ratios and

also in two different low-turbulence wind tunnels (Tu $\leqslant$ 0.1%); see also Section 6.3.2. Interestingly, the correlation study of Leehey and Hanson (1971), see also Blake (1986), extending down to $\mathrm{Re} = 3 \times 10^3$ for Tu = 0.04% ($\ell/d = 96$), shows, with increasing Re, a similar rapid drop in spanwise correlation as found in the present study (Figs. 3 and 12). However, the drop found by Leehey and Hanson occurs at a somewhat lower Reynolds number. The cause of this discrepancy is unclear. However, it is noted that the results of Leehey and Hanson are to some extent influenced by tiny vibrations of the cylinder. These vibrations may have had some triggering effect on the shear-layer instability, in similarity with an effective increase in Reynolds number (Gerrard, 1965; Norberg, 1987a).

On the first local maximum in R_{uu} ($\mathrm{Re} \simeq 0.3 \times 10^3$) it ought to be mentioned that the actual Reynolds number where it occurred was slightly dependent on the relative position of the hot-wire combination. The cylinder diameter in these measurements was $d = 3$ mm. At the standard position ($x/d = 0.4$, $y/d = 0.9$) a maximum correlation was found at $\mathrm{Re} \simeq 0.30 \times 10^3$. In passing, it can be noted (Fig. 12) that this hot-wire position produced correlation coefficients, for $s/d = 6.0$, in reasonable agreement with matching results using another diameter ($d = 6$ mm, $\mathrm{Re} \sim 2 \times 10^3$), despite the obvious violation of perfect geometrical similarity due to constant dimensions of the hot-wire combination. When at ($x/d = 0.7$, $y/d = 0.9$) the maximum in $R_{uu}(s/d = 6.0)$ occurred at $\mathrm{Re} = (0.29 - 0.30) \times 10^3$ and finally with the hot-wire combination at ($x/d = 2.5$, $y/d = 1.2$) it showed up at $\mathrm{Re} = (0.26 - 0.27) \times 10^3$. As is apparent, there was a slight decrease in the critical Re with increasing distance from the cylinder. Two reasons for this behavior are suggested. The first is that the wake transition scenario was somewhat affected by the presence of the hot-wire combination. As shown in Williamson and Roshko (1990) and Norberg (1994), a peak in base suction occurs at around $\mathrm{Re} \simeq 0.26 \times 10^3$, the peak being indicative of a finalization of the wake transition process. In addition, at around this particular Reynolds number of about 260, the near-wake shedding flow has a strong spanwise coherence (Williamson, 1996b). As the hot-wire combination was positioned closer to the cylinder, despite being outside the separated shear layers, there could had been some small alterations imposed on the vortex shedding process with the result of a delay in wake transition, a stabilizing effect, forcing the transition to occur at a higher Re. Unfortunately, there were no subsidiary measurements carried out to either confirm or reject this hypothesis. Another reason could be, at around these Reynolds numbers, that the sequence of spanwise ordering of velocity fluctuations in the wake has an hitherto unknown spatial variation. The subtle variations due to position might then be just a manifestation of the complexity of the wake transition process. It should be noted, however, that on the general appearance of the $R_{uu}(s/d = 6.0)$ versus Re there was no significant change due to the position of hot wires. In addition, the high level of correlation at around $\mathrm{Re} = (0.26 - 0.30) \times 10^3$ was largely unaffected by the position of hot wires, see Fig. 12.

As for the local minimum in R_{uu} ($\mathrm{Re} \simeq 1.6 \times 10^3$) it was noted that the actual Reynolds number for this minimum to show up was seemingly unaffected by the relative position of the hot wires. Presumably, the precise critical Re is related to the onset of observable shear-layer vortices, which has been reported to occur within the range Re = 1200–1800 (Prasad and Williamson, 1997a). As shown in Fig. 12, the correlation level was in general higher the more downstream the position of the hot wires, the effect being strongest at around the local minimum at $\mathrm{Re} \simeq 1.6 \times 10^3$. Here it can be inferred that the closeness to the mean point of primary vortex roll-up (or the mean wake closure point) has an effect of increasing the spanwise correlation. At around $\mathrm{Re} = 1.6 \times 10^3$, the mean wake closure occurs at $x/d = 2.3$ (Norberg, 1998), which is slightly upstream of the most distant hot-wire position in the present correlation study. Strong signatures of low-frequency pulsations in the near wake have been reported, especially at streamwise positions close to the wake closure point (Hanson and Richardson, 1968). Although not contributing largely to the fluctuating lift (Fig. 10), these low-frequency events do appear to have a significant spanwise correlation (Ferguson and Parkinson, 1967; Sonneville, 1976). The increase in correlation with increasing streamwise distance from the cylinder might also be connected to an influence of spanwise-correlated shear-layer oscillations, which, at these Reynolds numbers, presumably are initiated slightly upstream of the wake formation (Bloor, 1964). Nevertheless, the correlation results which are considered most representative for the fluctuating lift are those which were taken at the position closest to the cylinder.

Measured distributions of $R_{uu}(s/d)$ were adjusted to fit the weighted model function of Eq. (13), see Fig. 13. In Fig. 13(b), for $\mathrm{Re}/10^3 = 3.0$ and 5.1, the spanwise correlation lengths as found from the fitting procedure ($\Lambda/d = 12.3$ and 17.6, respectively) were considered to be overestimated. For very large separations, the resulting model functions did not exhibit the anticipated behavior of a rapid drop in correlation towards the cylinder end. To remedy this, the function R_{uu} was set to zero at a position two diameters from the end plate (at $s/d = 38$). The lengths reported in Fig. 3 were then obtained from a direct numerical integration of the measured function R_{uu} with this zero point added ($\Lambda/d = 10.4$ and 15.2, respectively).

As shown in Fig. 13(b), see also Fig. 12, a very rapid increase in spanwise correlation occurred in between Reynolds numbers 0.24×10^3 and 0.28×10^3. For $\mathrm{Re} = 0.24 \times 10^3$, the indicated spanwise correlation length was about 9.5 diameters, whereas a value of about $\Lambda/d = 29$ was found for $\mathrm{Re} = 0.28 \times 10^3$. As mentioned above, the highest spanwise correlation for $s/d = 6.0$ was found within $\mathrm{Re} = (0.26 - 0.30) \times 10^3$, the precise value being somewhat

dependent on the position of hot wires. The maximum spanwise correlation length was estimated to be approximately 30 diameters.

At $\mathrm{Re} = 0.24 \times 10^3$, the flow was in the wake transition regime (Williamson, 1996a) with a shedding flow that is expected to be highly disordered and spanwise fragmented due to the presence of a mix of mode A and B instability structures (Williamson, 1996b; Henderson, 1997). The spanwise correlation length found at $\mathrm{Re} = 0.24 \times 10^3$ is of the same order as twice the wavelength of the most unstable mode A instability (Barkley and Henderson, 1996). With a subsequent increase in Reynolds number, the mode B instability becomes the most prominent 3-D feature (Williamson, 1988b).

In Fig. 13(b), the peak in spanwise correlation found at $\mathrm{Re} = 5.1 \times 10^3$ is depicted; see also Norberg (1987a, 1989). The increased levels of correlation appeared to be most prominent for intermediate spanwise separations, at around 10–20 diameters. Similar elevated levels at intermediate separations are found also in the study of Leehey and Hanson (1971), albeit in their case for $\mathrm{Re} = 3.25 \times 10^3$; see Blake (1986).

Presumably, the mismatch in between present correlation results and those of Leehey and Hanson, however, similar in general appearance, has to do with differences regarding the process of shear-layer transition.

The complexity of the correlation function as found for lower Re seemed to disappear at a Reynolds number of about 8×10^3. Here (Fig. 13(b)) the correlation function could be rather well approximated as a simple exponential drop, Eq. (8). The correlation length of 5.3 diameters for $\mathrm{Re} = 8.0 \times 10^3$ is in reasonable agreement with previous measurements (Fig. 3). For higher Reynolds numbers, $\mathrm{Re} > 10^4$, the correlation lengths were calculated from the correlation function at $s/d = 2.2$ using the exponential drop as a model function ($d = 40$ mm). The level of correlation as well as the trend of a slow decrease in Λ/d with increasing Re are in general agreement with previous findings, see Fig. 3.

6. Final discussion

The shedding flow in relation to variations in Strouhal number (St), sectional lift coefficient ($C_{L'}$) and normalized spanwise correlation length (Λ/d) with Reynolds number (Re) is discussed further in this section.

6.1. Laminar shedding

Onset of vortex shedding occurs at $\mathrm{Re} = \mathrm{Re}_c \simeq 47$; e.g. see Dupin and Teissié-Solier (1928) and Norberg (1994). Obviously, it is also the onset of fluctuating lift. The onset can be characterized as a supercritical Hopf bifurcation, which as well as the resulting stable two-dimensional periodic shedding close to onset can be described by the Stuart–Landau equation (Provansal et al., 1987). A supercritical parameter may be defined:

$$\varepsilon = \frac{\mathrm{Re} - \mathrm{Re}_c}{\mathrm{Re}_c}. \tag{24}$$

Direct and indirect measurements for $\ell/d > 40$, approximately, show that the shedding flow close to onset is truly two-dimensional, regardless of the end conditions; see Williamson (1989), Lee and Budwig (1991) and Norberg (1994). However, to maintain this 2-D parallel shedding condition at even higher Reynolds numbers there has to be some slight manipulation at the cylinder ends (Williamson, 1996a). Within this laminar shedding regime, which can be made to persist up to about $\mathrm{Re} = 190$ (Williamson, 1996a), it is known from numerical simulations (Park et al., 1998) that the lift fluctuations are almost perfectly sinusoidal. Without end manipulation, e.g. using ordinary end plates, the onset of slanted shedding occurs at $\mathrm{Re} \approx 70$ (Norberg, 1994) corresponding to $\varepsilon \approx 0.5$. From the Stuart–Landau equation, close to onset of vortex shedding at $\varepsilon = 0$, the saturated shedding frequency f_S times the viscous time scale d^2/ν, the Roshko number, varies linearly with ε, i.e.,

$$f_S d^2/\nu = \mathrm{Ro} = \mathrm{Re} \times \mathrm{St} = A_0 + A_1 \times \mathrm{Re}. \tag{25}$$

A least-square fit to the combined St-data of Norberg (1987a, 1994), for $47 < \mathrm{Re} < 70$ gave ($A_0 = -3.976$, $A_1 = 0.2016$) with a mean absolute relative error of 0.3% (30 points).

Again from the Stuart–Landau equation, at least close to the onset, the limit-cycle amplitude of periodic velocity fluctuations in the flow is proportional to $\varepsilon^{1/2}$ (Schumm et al., 1994). Although not fully established theoretically, it seems that the sectional lift amplitude is linearly related to velocity fluctuations close to the cylinder. Consequently and to leading order a square-root dependency for the r.m.s. lift coefficient versus Re is expected, $C_{L'} \propto \varepsilon^{1/2}$; see also Gerrard (1997). Results from 2-D simulations within the laminar shedding regime, e.g. Park et al. (1998) and Posdziech and Grundmann (2000), support this initial square-root dependency. For higher Reynolds numbers a gradual change to a

linear variation is indicated. Based on published 2-D simulation data for $Re \leqslant 200$, see Table 5, the following approximate formula is suggested ($Re_c = 47$):

$$C_{L'} = \sqrt{\varepsilon/30 + \varepsilon^2/90}. \tag{26}$$

The constants have been adjusted towards the results that were considered the most reliable in terms in terms of accuracy and large enough calculation domain sizes, in particular those of Rosenfeld (1994), Beaudan and Moin (1994), Barkley and Henderson (1996), He and Doolen (1997), Park et al. (1998), Baek and Sung (1998), Zhang and Dalton (1998), Kravchenko et al. (1999) and Posdziech and Grundmann (2000); see Table 5 (Appendix B). For $Re = 100$ and 200, the two most frequent Reynolds numbers in 2-D simulation studies, the r.m.s. lift coefficients from Eq. (26) are 0.23 and 0.48, respectively. The mean absolute deviation between Eq. (26) and the extensive low-blockage $C_{L'}$-data of Posdziech and Grundmann (Oliver Posdziech, pers. comm.), for $47.5 \leqslant Re \leqslant 200$ (21 points), is 0.004.

Considering the whole laminar shedding regime the best representation of the St(Re) using only two constants seems to be the square-root functional relationship introduced independently by Fey et al. (1998) and Williamson and Brown (1998),

$$St = A + B/\sqrt{Re}. \tag{27}$$

A least-square fit to the combined parallel shedding data of Norberg (1987a, 1994) (92 points, $Re = 47 - 165$) gave ($A = 0.2663$, $B = -1.019$), with a mean absolute relative error of only 0.3% for the Strouhal number. The constants are virtually the same as found by Williamson and Brown ($A = 0.2665$, $B = -1.0175$) using the data of Williamson (1988a).

In summary, both Strouhal number and r.m.s. lift coefficient increases rapidly within the laminar shedding regime. At onset ($Re \simeq 47$) the Strouhal number is 0.12 ($Ro = 5.5$). At the highest attainable Reynolds number for two-dimensional flow, $Re \simeq 190$, the r.m.s. lift coefficient is $C_{L'} = 0.45$ (Posdziech and Grundmann, 2000). The corresponding Strouhal number is $St = 0.19$ (Miller and Williamson, 1994).

6.2. Wake transition

Onset of the first intrinsic three-dimensional instability, the mode A instability, occurs in between $Re = 160$ and 190, the precise value being somewhat dependent on the end conditions (Williamson, 1996a). The critical spanwise wavelength of mode A at its inception is about 4 diameters, see Williamson (1996a). As from this point and up to about $Re = 230$, the approximate onset of mode B (Williamson, 1988b), the shedding flow is expected to be highly disturbed, comprising a mix between mode A instability structures and large-scale, spot-like "vortex dislocations", in Williamson (1992) referred to as mode A*. Following Williamson (1996a), the natural wake transition follows the sequence (2-D → A* → B). For obvious reasons the change from 2-D to A* involves a dramatic decrease in the spanwise correlation of velocity fluctuations in the wake. It also involves a significant drop in shedding frequency and its associated spectral quality (Norberg, 1987a; Williamson, 1988a, 1996b). The sectional r.m.s. lift coefficient is expected to decrease in this process (Zhang et al., 1995).

In mode A*, the spanwise correlation length associated with near-wake velocity fluctuations can be expected to be of the same order as the wavelength of the most unstable mode A instability. The present measurements indicated a spanwise correlation length of about 7 diameters at the lowest attained Reynolds number, $Re = 230$, which is about twice this wavelength (Barkley and Henderson, 1996). As shown in Norberg (1994), there is, within $Re \simeq 165$ to $Re \simeq 230$, a relatively weak influence of the necessary aspect ratio to obtain independent global results. This implies (see also Roshko, 1954) a rather low spanwise correlation length for this initial, A*-dominated part of the wake transition regime, estimated here to be approximately 7 cylinder diameters, $\Lambda/d \approx 7$. Within flow state A* and with increasing Re, both Strouhal number (Williamson, 1996a) and r.m.s. lift coefficient (Zhang et al., 1995) increase.

With the inception of mode B ($Re \approx 230$), mode A being in a declining phase, there is a stabilization on the near-wake vortex shedding (Williamson, 1996b). With a subsequent increase in Re, mode B gradually becomes the dominant 3-D wake feature. During this process the spanwise correlation is expected to increase. The present experiments indicated a spanwise correlation length of about 9.5 diameters at $Re = 240$ rising to a maximum of about 30 diameters at $Re = 260$–300. As shown in Williamson (1996b), the shedding flow at $Re \simeq 260$ exhibits a remarkable high spanwise coherence, which is supported from the present measurements. It is also in conformity with the very large aspect ratios which are needed for independent results at around these Reynolds numbers (Norberg, 1994).

After the inception of mode B and with an increase in Re the r.m.s. lift coefficient continues to increase (Zhang et al., 1995). However, based on the simulations by Zhang et al., there seems to be a local maximum reached for $C_{L'}$ at around the same point where there is a peak in base suction (Williamson and Roshko, 1990), which also coincides with the re-introduction of an extremely high spectral quality of the shedding frequency, at $Re \simeq 260$ (Norberg, 1987a).

For wake-transitional flow, the following approximate linear variations for the r.m.s. lift coefficient are suggested, based on 3-D simulations by Zhang et al. (1995) and Zhang and Dalton (1998):

$$C_{L'} = \begin{cases} 0.43 \times (\mathrm{Re}/230) & (165 < \mathrm{Re} \leqslant 230), \\ 0.78 \times (\mathrm{Re}/260) - 0.26 & (230 < \mathrm{Re} \leqslant 260). \end{cases} \tag{28}$$

The shaded region in Fig. 2 for Re = 165–190 is supposed to reflect the ambiguity in $C_{L'}$ due to effects of various end conditions (Williamson 1996a) and the subcritical nature of the mode A instability (Barkley and Henderson, 1996).

For flow around a circular cylinder, it has to be mentioned that there has been no mention in the literature about the presence of distinct lift (and drag) pulsations during wake transition. Such events have been observed from simulations of transitional flows around sharp-edged cylinders, e.g. a normal flat plate (Balachandar et al., 1997) and a square cylinder (Sohankar et al., 1999). As suggested by Sohankar et al. (1999) these lift pulsations are due to a mismatch in phase between lift and shedding frequency variations, not found for the circular cylinder (Henderson, 1997). This mismatch in phase might be related to the separation line being fixed for a sharp-edged cylinder but not so for the circular cylinder.

6.3. Turbulent shedding

Based on previous measurements, e.g. Roshko (1954), Hama (1957), Bloor (1964), Gerrard (1978) and Unal and Rockwell (1988), the (time-mean position of) transition to turbulence in the wake reaches the formation region somewhere within $\mathrm{Re} \simeq 260$ to 300, presumably closer to Re = 260. Turbulent shedding conditions prevail for all higher Reynolds numbers.

6.3.1. Lift crisis

As from the onset of turbulent shedding and with increasing Re there seems to be an increasing disorder in the fine-scale three dimensionalities associated with the secondary and essentially streamwise-oriented vortices of type mode B (Williamson, 1996a). Conceivably, this increasing disorder is simply due to the increasing significance of inertial effects with increasing Re. However, at these rather low Reynolds numbers, viscous effects may still play a significant role for the vortex-shedding process (Roshko, 1993). As shown in Brede et al. (1996) the normalized circulation of the secondary mode B vortices (scaling with Ud) increases by as much as 50% between $\mathrm{Re} \simeq 300$ and Re = 500 (which is their highest attainable Re). This increase in secondary (essentially streamwise) circulation occurs probably at the expense of the primary (essentially spanwise) circulation associated with the roll-up of the von Kármán vortices (Mansy et al., 1994). Consequently, since the alternate roll-up is closely related to fluctuating lift, $C_{L'}$ drops with increasing Re.

Based primarily on the interrelation between base suction, vortex formation length and sectional r.m.s. lift it can be inferred that there is a drop in $C_{L'}$ with increasing Re already from $\mathrm{Re} \simeq 260$. Three-dimensional simulations indicate $C_{L'} \approx 0.5$ for Re = 300 (Zhang et al., 1995; Kalro and Tezduyar, 1997; Kravchenko and Moin, 1998). For $260 < Re \leqslant 1.6 \times 10^3$, also taking present experimental data (Table 3) into account, the following tentative formula is suggested:

$$C_{L'} = 0.045 + 1.05 \times (1 - \mathrm{Re}/1600)^{4.5}. \tag{29}$$

From Re = 260–300 to $\mathrm{Re} \simeq 1.6 \times 10^3$ there was an indicated rapid drop in the spanwise correlation length, from about 30 to 8 diameters (Section 5.3). The corresponding increase in Strouhal number is very small, only about 5% (Fig. 1). The present data suggests that a local minimum of the sectional r.m.s. lift coefficient occurs at $\mathrm{Re} \simeq 1.6 \times 10^3$, the indicated minimum value being $C_{L'} \simeq 0.045$. Local extreme values at around this particular Reynolds number also occur for other time-averaged quantities. In addition, the anti-correlation between fluctuating pressures at the shoulder positions of the cylinder (Fig. 7) and the spanwise correlation of lift-related velocity fluctuations (Fig. 12) reach local minima at around $\mathrm{Re} = 1.6 \times 10^3$. These facts taken together suggest that the lift-related shedding flow reaches a position of extreme weakness at around $\mathrm{Re} = 1.6 \times 10^3$; see also Gerrard (1978). However, the vortex shedding still persists and has a strong periodicity, the Strouhal number at $\mathrm{Re} = 1.6 \times 10^3$ being $\mathrm{St} \simeq 0.212$ (Norberg, 1994).

It is to be noted that from about Re = 270 to 1400 the total r.m.s. lift force on a large-aspect-ratio cylinder, proportional to $C_{L'} \times \mathrm{Re}^2 \times \sqrt{\Lambda/d}$ (Eqs. (3) and (7)), is indicated to be approximately constant. It seems appropriate to classify this remarkable behavior (and the subsequent very low r.m.s. lift coefficient at $\mathrm{Re} \simeq 1.6 \times 10^3$) as a *lift crisis*. The suggested variations for $C_{L'}$ and Λ/d (Appendix A) indicate that the corresponding increase in free-stream velocity with a factor of about 5 (1400/270 = 5.2) will only cause a $\pm 15\%$ variation in the total r.m.s. lift acting on the cylinder! In perspective, the total mean drag increases by about a factor 600 ($C_D \approx 1$).

The *lift crisis* may have some relation to the phenomenon described in Yokoi and Kamemoto (1992, 1993) as "spread spots". The spread spots are shown to have a close relationship with the rib-like secondary vortices of type B, which in turn are firmly connected to the von Kármán vortices (Bays-Muchmore and Ahmed 1993; Williamson, 1996a). It appears that there are feedback motions in between the ribs, the roll-up of primary (von Kármán) vortices and the process of flow separation from the cylinder, causing spanwise undulations of the separation line. At present, however, the reason for these spots to occur and their significance for fluctuating lift and its associated spanwise correlation are unclear.

6.3.2. Two turbulent shedding modes

The present results confirm the existence of two turbulent shedding modes within the so-called subcritical regime, first noted in Norberg (1987a). The following is a short account for a chain of possible reasons for such a mode change to occur as well as some descriptive characteristics.

As from the initiation of turbulent shedding and up to about $\mathrm{Re} = 5 \times 10^3$, the streamwise mean position of wake transition is rather fixed with respect to the cylinder, although being upstream of the mean position of wake closure (Bloor, 1964). It seems that, at these Re, the transition to turbulence in the wake is not due to a shear-layer instability, if so the position ought to be moving towards the cylinder with increasing Reynolds number. Instead, at these Re, it is suggested that the transition to turbulence has its origin in the near-wake development of the rib-like secondary vortices of type mode B. As such, a rib-like vortex structure is swept across the wake centreline, being on the upstream side of its associated von Kármán vortex within the connecting braid shear layer inside the formation region (Bays-Muchmore and Ahmed, 1993; Brede et al., 1996; Lin et al., 1996), there will be a rapid stretching of the structure itself which, in connection with possible interactions with the primary roll-up, leads to a rapid break-down into small-scale turbulence. It seems that mode B vortices also have some sort of a timing or regulating role for the vortex shedding process. The spectral quality of the shedding frequency, from about $\mathrm{Re} = 260$ to 5.1×10^3, is extremely high (Norberg, 1987a). Interestingly, this *high-quality* mode of turbulent shedding appears not to be present for flow around sharp-edged cylinders with fixed separation lines (Norberg, 1993b). Presumably, for the circular cylinder, the feedback mechanism responsible for this stabilization of the shedding frequency has to do with the above-mentioned link in between the rib-like vortices, the developing von Kármán vortices and ultimately with the separation process.

The Reynolds number for extreme shedding weakness, $\mathrm{Re} \simeq 1.6 \times 10^3$, coincides with the point where shear-layer vortices show up as important ingredients in the near wake (Prasad and Williamson, 1997a). Interestingly, at around this Re, see Norberg (1998), the indicated (estimated) position of transition to turbulence in the separated shear layers (Roshko, 1993; Williamson, 1996a) coincides approximately with the streamwise position of wake closure. However, the actual wake transition occurs further upstream, presumably, as suggested above, triggered by the mode B vortices. Nonetheless, the shear-layer vortices will introduce additional shear stresses to the near wake and, to balance this (Roshko, 1993), the formation region shrinks and the base suction increases (Linke, 1931; Bloor 1964; Norberg, 1994, 1998). Consequently, the sectional $C_{L'}$ increases, at first rather slow but as shown in Figs 2 and 8 there is a subsequent very rapid increase in between $\mathrm{Re} = 5 \times 10^3$ and 7×10^3.

The presence of shear-layer vortices of significant strength within the wake formation region opens the possibility for direct interactions with the mode B vortices, already present within this region (Brede et al., 1996). As outlined in Norberg (1998), it is suggested that an interaction process of importance for the vortex shedding (and thus fluctuating lift) occurs in between spanwise length scales of these two types of (secondary) vortices, λ_z^{SL} and λ_z^B.

With an increase in Re the indicated time-mean value for λ_z^{SL} is approaching the corresponding value for λ_z^B (Norberg, 1998). During the same process the indicated mean position of transition in the shear layers moves upstream, closer to the observed (Bloor, 1964), actual mean position of wake transition, which presumably is mode-B related. Conceivably, this increases the mutual coupling in between these secondary vortical structures with the result of an increased spanwise correlation of near-cylinder velocity fluctuations. With a subsequent further increase in Reynolds number, there will eventually be a concurrence in between the mean values of λ_z^{SL} and λ_z^B. The analysis in Norberg (1998) indicates that this resonant, matching condition ($\lambda_z^{SL} = \lambda_z^B \approx 0.8 \times d$) occurs at $\mathrm{Re} \simeq 5 \times 10^3$, which then is in agreement with the peak in spanwise correlation found at around this particular Reynolds number (Fig. 12). In addition, at $\mathrm{Re} \simeq 5 \times 10^3$, the indicated streamwise position of shear-layer transition equals the corresponding position of the actual wake transition (Bloor, 1964; Norberg, 1998), about 1.1 diameters downstream of the cylinder axis. With a subsequent increase in Re, it is now the shear-layer vortices that trigger the wake transition, introducing a random forcing on the development of the regulating mode B vortices and subsequently also on the primary roll-up. At the transitional Reynolds number of about 5×10^3, the harmony between the development of mode B and von Kármán vortices is lost, causing spanwise undulations of the formation length, a decrease in the spectral quality of the shedding frequency and a decrease in spanwise correlation. This is the inception of the *low-quality* mode of turbulent shedding.

With increasing Re in the low-quality mode, the wake transition, now being governed primarily by a Kelvin–Helmholtz instability mechanism, moves further and further upstream, causing more and more disruptions and random forcing to the vortex-shedding process. Occasionally these disruptions lead to random-positioned vortex dislocations along the span. As suggested in Norberg (1993a) the local sectional lift amplitude during time periods of such a vortex dislocation is very low. Within the low-quality mode the fluctuating lift exhibits a characteristic amplitude modulation (Fig. 9(b)), high lift amplitudes being associated with strong vortex shedding where von Kármán vortices are rolling up close to the cylinder with a significant spanwise correlation; for low amplitudes the shedding is weak, the vortex formation region elongated and presumably the spanwise correlation of lift-related flow is much lower. It is thus conjectured that the phenomenon of distinct lift modulation (''beating''), characteristic for the low-quality mode, is due to the randomness being imposed on the formation of von Kármán vortices by the transition to turbulence in the separating shear layers.

The change-over from the high-quality shedding mode displaying a fairly regular vortex shedding and associated fluctuating lift amplitudes (Fig. 9(a)) with only minor spanwise undulation of the developing von Kármán vortices to the low-quality shedding mode displaying characteristic lift amplitude modulation (Fig. 9(b)), significant spanwise undulations and occasional but characteristic vortex dislocations, appears to be fully completed at around $\mathrm{Re} = 8 \times 10^3$ (Norberg, 1993a, 1998). In between $\mathrm{Re} \simeq 6 \times 10^3$ and 8×10^3 there is a plateau-like behavior of the base suction versus Re (Norberg, 1994). This ''kink'' in base suction is believed to be just another manifestation of the change-over between the high- and low-quality shedding modes (Norberg, 1998).

Some differences between the high- and low-quality modes are depicted in Fig. 14. In the high-quality mode (left, $\mathrm{Re} = 3 \times 10^3$) the upper separated shear layer can be seen to dip down towards the wake centerline. This was a characteristic and regular feature for this mode and is believed to be caused by suction actions from mode B vortices when being drawn across the wake centerline along with its associated von Kármán vortex. Being on the upstream side of the von Kármán vortex this cross-over of mode B vortices gives a signature of a local maximum in the r.m.s. streamwise velocity (u') along the wake centerline, upstream of the local maximum associated with (primary) vortex formation (Norberg, 1998). For $\mathrm{Re} = 3 \times 10^3$, these two local maxima occur at about 1.4 and 2.1 diameters downstream of the cylinder axis. In the low-quality mode (right, $\mathrm{Re} = 8 \times 10^3$), only one local maximum of u' is present along the wake centerline, here at $x/d = 1.6$. Within this mode the formation of mode B vortices is disturbed by the transition to turbulence and the upstream peak deteriorates to an inflexional point. At the exposure time for $\mathrm{Re} = 8 \times 10^3$ in Fig. 14, the shedding is within a period of strong vortex shedding. An example of sectional flow appearance within a period of weak vortex shedding, possibly during a near-wake vortex dislocation, is shown in Norberg (1993a).

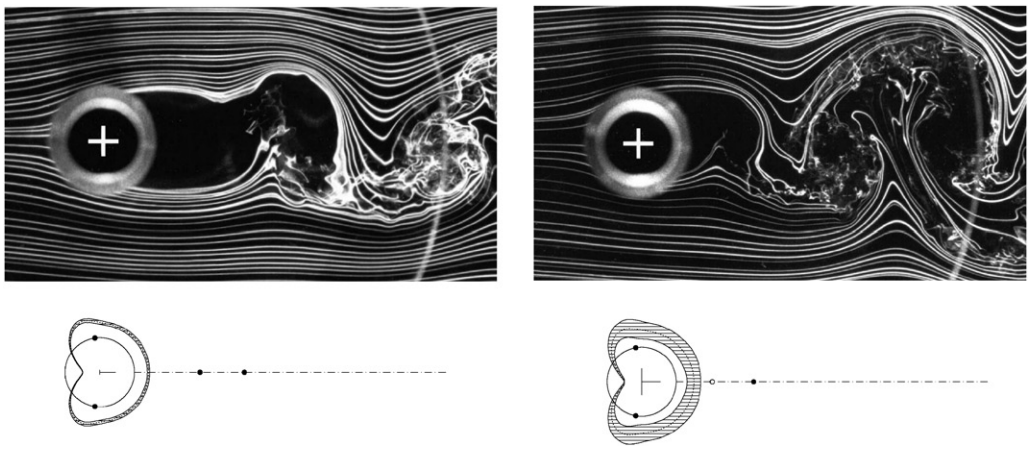

Fig. 14. Illustration of turbulent shedding modes. Left: $\mathrm{Re} = 3.0 \times 10^3$ (high-quality mode); Right: $\mathrm{Re} = 8.0 \times 10^3$ (low-quality mode). Upper: smoke-wire visualizations (Norberg, 1993a); Lower: mean pressure distribution C_p (dotted) with shaded area corresponding to $\pm 2 \times C_{p'}$, horizontal line from origin represents pressure C_D and vertical line from origin $\pm 2 \times C_{L'}$, the cylinder diameter being two units. Filled circles on cylinder surface are indicated separation points (max. $C_{p'}$); filled circles along wake centerline (line-dotted) depict local maxima for r.m.s. of streamwise velocity fluctuations, unfilled circle an inflexional point (Norberg, 1998).

6.3.3. Closure

At around $\mathrm{Re} = 10^4$ the transition in the separated shear layers has reached a mean position corresponding to just above the base point of the cylinder (Linke, 1931; Bloor 1964; Norberg, 1998). As from about this Re, the variations of $C_{L'}$ and Λ/d with increasing Re slow down (Figs. 2 and 3).

At $\mathrm{Re} = 1.6 \times 10^5$ the Strouhal number passes through a minimum value of $\mathrm{St} \simeq 0.186$, while, as depicted in Fig. 1, the relative shedding bandwidth passes through a maximum. The relative shedding bandwidth at this point is about 50 times higher than just the before the change-over to low-quality shedding. The associated sectional r.m.s. lift coefficient is about $C_{L'} = 0.51$ (Fig. 2). As relative shedding bandwidth and lift modulation are interrelated, the amplitude modulation of fluctuating lift is supposed to be at its largest magnitude at around this Re; see also Szepessy and Bearman (1992). At these high Re, the sectional r.m.s. drag coefficient also reaches appreciable magnitudes, the ratio $C_{L'}/C_{D'}$ being approximately 3 at $\mathrm{Re} = 10^5$ (Batham, 1973; Sonneville, 1976; Taniguchi and Miyakoshi, 1990). Moreover, at $\mathrm{Re} \simeq 1.6 \times 10^5$, due to the closeness of transition in the separated shear layers, the first signs of a reattachment behavior becomes visible in the measured r.m.s. pressure distributions, at $\varphi \simeq 105^\circ$ (Fig. 5). With a subsequent increase in Re, the build-up to a fully reattached flow continues, the position of laminar separation moves downstream, the wake narrows and the Strouhal number increases and finally at around $\mathrm{Re} = 2.3 \times 10^5$ there is a rapid fall in both C_D and $C_{L'}$ when entering the critical regime (Fig. 8).

Based primarily on present sectional $C_{L'}$-data, see Fig. 2, the following empirical $C_{L'}$-functions, for Reynolds numbers from $\mathrm{Re} = 1.6 \times 10^3$ to 2.2×10^5, are suggested:

$$C_{L'} = \begin{cases} 0.045 + 3.0 \times [\log(\mathrm{Re}/1600)]^{4.6} & (1.6 < \mathrm{Re}/10^3 \leqslant 5.4), \\ 0.52 - 0.06 \times [\log(\mathrm{Re}/1600)]^{-2.6} & (5.4 < \mathrm{Re}/10^3 \leqslant 220). \end{cases} \tag{30}$$

In closure, it needs to be pointed out that all hitherto published 3-D simulation results on $C_{L'}$ (Table 6, Fig. 2) are extracted from spanwise-averaged lift data. For unclear reasons the unsteady coefficients have been time-averaged *after* a process of spanwise averaging (and not the other way around). As the shedding flow at turbulent conditions is supposed to be homogeneous in the spanwise direction with a limited spanwise correlation, a spanwise averaged r.m.s. lift coefficient will ultimately drop to zero with a subsequent increase in the spanwise dimension [Eq. (7)]. Obviously, the *sectional* r.m.s. lift coefficient does not exhibit this behavior. Nevertheless, the achievements in this area have been promising and have to a certain extent increased our knowledge of intrinsic lift-related flow phenomena. For instance, the simulations of Henderson (1997) for $\mathrm{Re} = 1000$, which are not claimed to be fully resolved in all parts of the wake, show spanwise flow evolutions and associated lift signals, which, in experiments, are typical for much higher Re with low-quality shedding (Henderson, 1998). Also the numerous 3-D simulation studies carried out for $\mathrm{Re} = 3.9 \times 10^3$ show a near-wake behavior of velocity fluctuations, which, also from experiments (Norberg, 1998), is characteristic for the high-Re, low-quality mode of turbulent shedding (pers. comm., Michael Breuer, Jochen Fröhlich, Arthur Kravchenko; also see Breuer, 1998; Fröhlich et al., 1998; Kravchenko and Moin, 1998). The mismatch on the effective global Reynolds number may be related to numerical dissipation effects due to insufficient spatial resolution, if so most probable within the vortex formation region where the assumed subtle *three-dimensional* process of wake transition and mode change occur. Also, limitations on the spanwise dimension may have had some influence, see Table 6.

7. Conclusions

Sectional root-mean-square (r.m.s.) lift coefficients have been estimated using a technique based on integration of the distribution of r.m.s. pressure around the circumference and simultaneous measurement of fluctuating pressures at the shoulders of the cylinder. In these measurements the Reynolds number range is from about $\mathrm{Re} = 0.7 \times 10^3$ to 2.1×10^5. Between Reynolds numbers 1.6×10^3 and 20×10^3 an approximate 10-fold increase in the sectional r.m.s. coefficient is indicated, from about $C_{L'} = 0.045$ to 0.47. A maximum sectional r.m.s. lift coefficient occurs at the upper end of the tested Reynolds number range, the value $C_{L'} = 0.52$ being in overall agreement with previous experiments.

Coefficients of spanwise correlation, based on near-cylinder velocity fluctuations just outside of the separated shear layers, have been measured from about $\mathrm{Re} = 0.23 \times 10^3$ to 75×10^3. At $\mathrm{Re} \simeq 230$, the approximate onset Re for the mode B instability, the one-sided spanwise correlation length (Λ) is about the twice the wavelength of the most unstable mode A instability, $\Lambda/d \approx 7$. Up to $\mathrm{Re} = 260$–300 the spanwise correlation increases dramatically, the indicated peak value being $\Lambda/d \approx 30$. Apart from a local maximum at $\mathrm{Re} \simeq 5.1 \times 10^3$, $\Lambda/d \approx 15$, there is then a gradual decrease in the spanwise correlation length with increasing Reynolds number, a value of about 3 diameters being indicated at $\mathrm{Re} = 75 \times 10^3$, in accordance with previous experiments.

The experiments provide further evidence for a fundamental change in mode of shedding in between $\mathrm{Re} = 5 \times 10^3$ and 8×10^3 (high- and low-quality mode of turbulent shedding, respectively). It is conjectured that the phenomenon of distinct lift amplitude modulation for $\mathrm{Re} > 6 \times 10^3$, approximately, is due to the randomness imposed on the formation of von Kármán vortices by the transition to turbulence in the separated shear layers.

Note added in proof

Some interesting new results from numerical experiments have recently been published. For instance, Posdziech and Grundmann (2001) report results on the spanwise-averaged r.m.s. lift coefficient for $\mathrm{Re} = 195$–330. Their results using different relative spanwise dimensions, confirm the finding of the present paper that there is a peak in spanwise correlation of fluctuating *sectional* lift forces at around $\mathrm{Re} = 0.28 \times 10^3$ (Figs. 3, 12 and 13).

Appendix A. Empirical functions

Suggested empirical functions for the Reynolds number dependence of Strouhal number (St), sectional r.m.s. lift coefficient ($C_{L'}$) and normalized spanwise correlation length (Λ/d), for Reynolds numbers $\mathrm{Re} = 47$ to 3×10^5, are summarized in Table 4. As with all empirical functions, they are open for re-evaluation when more data has been collected.

Appendix B. Review on numerical simulations

In the majority of previous numerical studies with results on fluctuating lift the main interest has been on introduction of new computational techniques and code validation. Results are often reported only for a single

Table 4
Summary of empirical functions

1. Strouhal number		
Re	$\mathrm{St} \simeq$	
$47 - 190$	$0.2663 - 1.019/\sqrt{\mathrm{Re}}$	
$165 - 260$	$-0.089 + 22.9/Re + 7.8 \times 10^{-4} \times Re$	
$260 - 325$	0.2016	
$325 - 1.6 \times 10^3$	$0.2139 - 4.0/Re$	
$1.6 \times 10^3 - 1.5 \times 10^5$	$0.1853 + 0.0261 \times \exp(-0.9 \times x^{2.3})$	$x = \log(\mathrm{Re}/1.6 \times 10^3)$
$1.5 \times 10^5 - 3.4 \times 10^5$	$0.1848 + 8.6 \times 10^{-4} \times (\mathrm{Re}/1.5 \times 10^5)^{4.6}$	
2. Sectional r.m.s. lift coefficient		
Re	$C_{L'} \simeq$	
$47 - 190$	$(\varepsilon/30 + \varepsilon^2/90)^{1/2}$	$\varepsilon = (Re - 47)/47$
$165 - 230$	$0.43 \times (\mathrm{Re}/230)$	
$230 - 260$	$0.78 \times (\mathrm{Re}/260) - 0.26$	
$260 - 1.6 \times 10^3$	$0.045 + 1.05 \times (1 - \mathrm{Re}/1.6 \times 10^3)^{4.5}$	
$1.6 \times 10^3 - 5.4 \times 10^3$	$0.045 + 3.0 \times x^{4.6}$	$x = \log(\mathrm{Re}/1.6 \times 10^3)$
$5.4 \times 10^3 - 2.2 \times 10^5$	$0.52 - 0.06 \times x^{-2.6}$	$x = \log(\mathrm{Re}/1.6 \times 10^3)$
$2.2 \times 10^5 - 3.4 \times 10^5$	$0.09 + 0.43 \times \exp[-10^5 \times (\mathrm{Re}/10^6)^{10}]$	
3. One-sided spanwise correlation		
Re	$\Lambda/d \approx$	
$47 - 190$	∞	
$165 - 285$	$11.5 \times [1 - \mathrm{erf}(\eta)] + 7.0$	$\eta = 22 \times (\mathrm{Re}/250 - 1)$
$285 - 1.5 \times 10^3$	$7.6 \times (\mathrm{Re}/1.5 \times 10^3)^{-0.82}$	
$1.5 \times 10^3 - 1.72 \times 10^3$	7.6	
$1.72 \times 10^3 - 5.1 \times 10^3$	$7.6 \times (\mathrm{Re}/1.72 \times 10^3)^{0.60}$	
$5.1 \times 10^3 - 8.0 \times 10^3$	$14.6 \times (\mathrm{Re}/5.1 \times 10^3)^{-2.3}$	
$8.0 \times 10^3 - 2.4 \times 10^5$	$2.6 \times (\mathrm{Re}/2.4 \times 10^5)^{-0.20}$	
$2.4 \times 10^5 - 3.0 \times 10^5$	$1.4 \times (\mathrm{Re}/3.0 \times 10^5)^{-2.7}$	

Table 5
Two-dimensional simulations of fluctuating lift (Re < 500)

Study	Re	H/d	X_u/d	X_d/d	$N/10^3$	$C_{L'}$(Re)		G:M:V
						100	200	
Jordan and Fromm (1972)	100/400	188	94	94	12	0.19	–	O:FD:$\psi\omega$
Smith and Brebbia (1977)	100	12	8.4	22	0.51	.14–.31	–	R:FE:$\psi\omega$
Swanson and Spaulding (1978)	100	135	68	68	2.4	0.24	–	O:FD:PV
Gresho et al. (1984)	50–400	8.8	4.6	16	1.8	0.52	0.74	R:FE:PV
Lecointe and Piquet (1984)	200	40	20	20	3.1	–	.50/.35	O:FD:$\psi\omega$
Braza et al. (1986)	100/200	115	57	57	13	0.21	0.55	O:FV:PV
Borthwick (1986)	40–400	80	40	40	8.2	0.18	0.43	O:FD:$\psi\omega$
Karniadakis (1988)	200	10	5	40	?	–	0.48	R:SE:PV
Lecointe and Piquet (1989)	140/200	80/110	40/55	40/55	23/109	–	0.42	O:FD:$\psi\omega$
Benson et al. (1989)	100/200	80,5	40	40	17	0.27	0.46	Q:DV:$\psi\omega$
Dougherty et al. (1989)	80	100	50	50	8.4	–	–	O:FD:PV
Dougherty et al. (1989)	200	50	25	50	9.0	–	0.50	C:FD:PV
Engelman and Jamnia (1990)	100	16	8.0	25	14	0.26	–	R:FE:PV
Franke et al. (1990)	50–300	40	20	20	8.3–26	–	0.46	O:FV:PV
Rogers and Kwak (1990)	200	20	10	10	6.0	–	0.46	O:FD:PV
Tezduyar and Shih (1991)	100	16	8.0	25	4.8	0.29	–	R:FE:PV
Tabata and Fujima (1991)	100	15	7.5	22	2.3	0.26	–	R:FE:PV
Behr et al. (1991)	100	16	8.0	25	4.8	0.23	–	R:FE:$\psi\omega$
Sa and Chang (1991)	50–200	43	22	22	2.6	0.17	0.24	O:FD:$\psi\omega$
Li et al. (1991)	45–300	10	5.0	20	0.83	0.29	–	R:FE:PV
Li et al. (1992)	100	10	5.0	20	2.6	0.24	–	R:FE:PV
Slaouti and Stansby (1992)	100/200	50,5.5	25	25	?	0.28	0.50	Q:DV:$\psi\omega$
Hwang and Lin (1992)	100/200	18	9.3	18	6	0.27	0.42	C:FD:PV
Meneghini and Bearman (1993)	200	50	25	25	23	–	0.54	O:DV:$\psi\omega$
Stansby and Slaouti (1993)	60–180	200	100	100	13	0.24	–	O:DV:PV
Anagnostopoulos (1994)	99–130	6.7	3.8	20	2.2	0.19	–	R:FE:$\psi\omega$
Rosenfeld (1994)	200	61	30.5	30.5	263	–	0.48	O:FV:PV
Lin and Wu (1994)	46–200	20	10	10	5.1	0.25	0.49	O:FV:PV
Beaudan and Moin (1994)	80/100	300	150	150	39/51	0.24	–	O:FD:PV
Behr et al. (1995)	100	32	8.0	22	9.7	0.26	–	R:FE:PV
Zhang et al. (1995)	40–300	12	6.0	16	21	0.25	0.53	C:FD:PV
Newman and Karniadakis (1995)	200	25	12.5	30	5.9	–	0.51	C:SE:PV
Anagnostopoulos et al. (1996)	106	20	5.0	20	6.5	–	–	R:FE:$\psi\omega$
Lu et al. (1996)	100	25	12.5	12.5	23	0.22	–	O:FS:PV
Blackburn and Henderson (1996)	250	25	12.5	25	5.5	–	–	C:SE:PV
Newman and Karniadakis (1996)	100	25	12.5	30	$\simeq 7$	0.24	–	C:SE:PV
Lu and Dalton (1996)	185	50	25	25	131	–	–	O:FD:PV
Barkley and Henderson (1996)	190	56	16	25	22	–	–	R:SE:PV
Gunzburger and Lee (1996)	60/80	10	5.0	15	3.7	–	–	R:FE:PV
Cheng et al. (1997)	200	100	50	50	10	–	0.48	O:FV:PV
Tang and Aubry (1997)	56–200	2^4	10^4	10^4	102	0.21	0.45	O:FV:$\psi\omega$
Lilek et al. (1997)	100	32	16	20	18	0.24	–	R:FV:PV
Zhang and Dalton (1997)	200	50	25	25	21	–	0.38	O:FD:$\psi\omega$
Kalro and Tezduyar (1997)	300	15	7.5	30	4.7	–	–	R:FE:PV
Kjellgren (1997)	100	16	7.6	23	5.3	0.19	–	R:FE:PV
He and Doolen (1997)	50–150	111	55	55	44	0.23	–	O:LB:PV
Gharib et al. (1997)	100	–	–	–	–	0.23	–	–:DV:$u\omega$
Piñol and Grau (1998)	60/100/200	25	5.0	20	16	0.19	0.42	R:FD:$\psi\omega$
Baek and Sung (1998)	110	56	28	20	32	–	–	C:FD:PV
Jameson and Martinelli (1998)	150/200	32	16	16	66	–	0.45	O:FD:PV
Olinger and Alexandrou (1998)	100	8.0	4.0	20	1.9	0.26	–	R:FE:PV
Persillon and Braza (1998)	100–300	16.5	9.8	22	22	0.27	0.56	R:FV:PV
Park et al. (1998)	60–160	100	50	20	39	0.24	–	C:FD:PV
Zhang and Dalton (1998)	200	100	50	50	20.5	–	0.48	O:FS:PV
Jia (1998)	200	50	25	25	10	–	0.44	O:FD:PV

Table 5 (*continued*)

Study	Re	H/d	X_u/d	X_d/d	$N/10^3$	$C_{L'}$(Re)		G:M:V
Liu et al. (1998)	100–200	??	??	??	66	0.24	0.49	O:FD:PV
Kravchenko et al. (1999)	80/100	120	60	60	32	0.22	–	O:FD:PV
Zhou et al. (1999)	100/200	125	62	62	20	0.22	0.59	O:DV:$\psi\omega$
Patnaik et al. (1999)	100/200	20	5.0	30	2.1	0.35	0.65	R:FE:PV
Bertagnolio (1999)	200	16	5.0	20	26	–	0.50	R:FD:PV
Visbal and Gaitonde (1999)	100	100	50	50	31	0.22	–	O:FD:PV
Su and Kang (1999)	100	20?	20?	40?	19	0.24	–	R:FV:PV
Farrant et al. (2000)	200	20	16	14	19	–	0.51	R:FE:PV
Posdziech and Grundmann (2000)	47.5–330	140	70	50	19	0.23	0.48	C:SE:PV

Table 6
Three-dimensional simulations of fluctuating lift ($\mathrm{Re} < 10^5$)

Study	Re	H/d	X_u/d	X_d/d	L_z/d	C_s[a]	$C_{L'}$
Batcho and Karniadakis (1991)	500	6?	3?	13?	1.57	0	0.2[b]
Kato and Ikegawa (1991)	10^4	10	5	15	2.0	0.1	0.27
Izumi et al. (1994)	1100	30	15	15	6.0	0	0.26
Beaudan and Moin (1994)	3900	150	75	75	3.14	0	0.07
Zhang et al. (1995)	140–300	12	6	16	6/9	0	0.26–0.55
Mittal and Balachandar (1995)	525	15	7.5	7.5	1.0	0	0.45
Henderson and Karniadakis (1995)	1000	44	22	48	50.3	0	0.2
Henderson (1997)	1000	64	32	48	25.1	0	0.3[b]
Lu et al. (1997a)	10^4	25	12.5	12.5	2.0	0.1	0.46
Lu et al. (1997b)	$(0.3, 2.0, 4.4) \times 10^4$	49	24.5	24.5	2.0	0.1	(0.48,0.38,0.42)[b]
Kalro and Tezduyar (1997)	300/800	15	7.5	30	4.0	0	0.6/0.4[b]
Kalro and Tezduyar (1997)	10^4	15	7.5	30	4.0	0.15	0.3[b]
Kravchenko and Moin (1998)	300	60	30	30	6.28	0	0.40
Fröhlich et al. (1998)	3900	30	15	15	3.14	0.1	0.3[b]
Persillon and Braza (1998)	100–300	16.5	9.8	22	2.25	0	0.27–0.7
Zhang and Dalton (1998)	100	43	21	21	11	0	0.23
Zhang and Dalton (1998)	200	100	50	50	15	0	0.43
Evangelinos and Karniadakis (1999)	1000	44	22	69	12.6	0	0.099

[a] Smagorinsky constant in subgrid scale model, a zero means that no modeling is applied.
[b] From time series, value has been estimated.

Reynolds number, the most common for 2-D flow being $\mathrm{Re} = 100$, 200, see Table 5. The unconfined cylinder is mostly addressed and for physical realization of this canonical case a sufficiently large domain is required (upstream, sideways, downstream and spanwise). A high accuracy demands for a sufficiently fine spatial resolution, in all parts of the domain, and as the flow under consideration is time dependent there is also a need for a sufficiently fine time resolution. Even if such a fine spatio-temporal resolution is fulfilled, the required necessary minimum domain distances (for realization) will be dependent on the Reynolds number and the applied boundary conditions, respectively.

Tables 5 and 6 are not exhaustive regarding all various numerical parameters or factors which may have an influence on local and global results. For instance, time step, boundary conditions and parameters related to spatial resolution are not included. The reader is referred to specific references for more details. For 2-D only studies with $\mathrm{Re} < 500$ are included whereas the restriction for 3-D is $\mathrm{Re} < 10^5$.

The tables contain some parameters and abbreviations, explained as follows. Parameter H is the width of the domain perpendicular to the oncoming flow (in the plane containing the cylinder axis) whereas X_u and X_d are the distances from the cylinder axis to the upstream and downstream boundary, respectively. Usually, the inverse of H/d is referred to as blockage ($\beta = d/H$). In Table 6, also the spanwise dimension L_z and the Smagorinsky constant C_s are included ($C_s = 0$ means that no subgrid scale model is used). For all simulations in Table 6 a periodic boundary condition is applied at the cylinder ends, L_z then represents the spanwise distance over which the simulated flow is periodic, except in Persillon and Braza (1998) who use Neumann boundary conditions. The last column in Table 5 provides (as a sequence G:M:V) the grid/domain type (G), solution method (M) and solution variables (V). For grid/domain types, O refers to a polar or

O-grid (for such grids H, X_u and X_d are coupled, $X_u = X_d = H/2$); R refers to a rectangular domain; C to a domain which is elliptic or polar upstream and rectangular downstream (C-grid/domain) and finally Q is a domain which has a polar grid overlapping a smaller rectangular grid extending downstream. For solution methods, FD means solutions based on finite differences, FE finite elements, FV finite volumes, SE spectral elements, DV discrete vortices; LB is the lattice Boltzmann method; FS is a combined finite differences/spectral approximation. For variables, $\psi\omega$ means a solution based on streamfunction ψ and vorticity ω whereas PV means primitive variables (velocity components u and v). The total number of grid or nodal points is denoted N and it represents the most refined case. For SE-methods using high-order polynomials representation within each spectral element, N has been estimated as $k \times p^2$ where k is the number of spectral elements and p is the polynomial order.

Considering the upstream boundary, the standard procedure is to apply a uniform free stream condition ($u = U$, $v = w = 0$). This means that X_u/d cannot be chosen too small. In Sohankar et al. (1995), for 2-D flow around a square-section cylinder, the necessary value for obtaining independent results on r.m.s. lift is $X_u/d \approx 10$ (Re = 100).

On the necessary lateral dimension parameter H/d it has to be emphasized that this parameter, apart from Reynolds number, also is dependent on the domain type and the applied boundary conditions. For polar grids and unless special efforts are put on employing physically sound far-field boundary conditions on the upstream and downstream arcs, it seems that the outer boundary limit, for laminar shedding conditions, has to be placed at least 30 diameters from the cylinder center ($H/d > 60$), e.g., see Rosenfeld (1994), Beaudan and Moin (1994) and Kravchenko and Moin (1998). For domains of the R- and C-type there will be a true blockage effect when the cross-stream velocity component (v) is set to zero at lateral boundaries (for such cases H/d in Table 5 has been underlined, except for Anagnostopoulos (1994) where results have been adjusted for blockage). In Tezduyar and Shih (1991) the effect of changing the lateral boundary conditions from a symmetry condition, simulating "frictionless" confining walls ($\partial u/\partial y = 0$, $v = 0$) to a tow tank, free-stream condition ($u = U$, $v = 0$) is investigated for Re = 100. On r.m.s. lift they report a negligible influence with $H/d = 16$. Behr et al. (1995) present a study on the influence of H/d for $X_u/d = 8$ and $X_d/d = 22.5$ (rectangular domain, Re = 100). On r.m.s. lift, using symmetry conditions, it is indicated that $H/d > 24$ is needed to obtain independent results. Barkley and Henderson (1996), using a rectangular domain with tow tank conditions, find $H/d \geqslant 44$ to be necessary for independent global results (Re = 190). Posdziech and Grundmann (2000) use a C-domain with $H = 2 \times X_u$, $X_d/d = 50$ and tow tank conditions, and they find, for Re = 200, after successive domain extensions combined with systematic resolution tests, that $H/d \geqslant 80$ (approx.) is needed to obtain r.m.s. lift within the percentage level.

The required downstream distance X_d/d is very much dependent on the applied outlet boundary condition. In Behr et al. (1991) both a Neumann and a traction-free condition (Tezduyar and Shih, 1991) is tested for $X_d/d = 2.5 - 25$ ($H/d = 16$, $X_u/d = 8$). With the Neumann condition the necessary distance is $X_d/d \approx 20$, whereas for the more physical traction-free condition the critical distance decreases to $X_d/d \approx 10$. On the necessary downstream distance X_d/d the convective outlet condition (Lilek et al., 1997; Baek and Sung, 1998; Park et al., 1998; Kravchenko and Moin, 1998) seems to perform in a similar manner as the traction-free condition; see also Sohankar et al. (1998).

For a specified calculation domain, even when using an efficient numerical method, it is necessary to carry out grid refinements. However, in many cases and for reasons of computational cost, it has not been fully demonstrated that solutions are actually grid-independent. One extensive study on refinement tests is by Rosenfeld (1994). Here a polar grid with $H/d = 61$ is tested for convergence at Re = 200 (Table 5). On the outer boundary a uniform flow is prescribed, except in the wake region where Neumann-type boundary conditions are specified. The number of time steps per shedding period is 800. The solutions are formally second order in space, demonstrated by successive grid refinements. By extrapolating to zero mesh sizes a lift amplitude of 0.676 is reported ($C_{L'} = 0.478$). In the study of Posdziech and Grundmann (2000) the limiting lift amplitude for Re = 200 is 0.669 ($H/d = 240$, $X_u/d = 120$, $X_d/d = 50$, $k = 186$, $p = 10$). For further information on the effects of spatial resolution, effective grid clustering, grid refinements, etc. the reader is referred to specific references in Tables 5 and 6.

In 3-D simulations for Reynolds numbers with intrinsic 3-D flow, Re > 190 approximately, the relative spanwise dimension, L_z/d, becomes a most important parameter, see Table 6. As pointed out in Henderson (1997), L_z/d (using periodic spanwise boundary conditions) cannot be compared directly with aspect ratio ℓ/d in experiments. Lift fluctuations with inherent 3-D flow may also have a complex time dependency, the nondimensional integration time for taking out the r.m.s. lift then becomes a parameter of some importance. Recent studies, e.g. Henderson (1997) and Ma et al. (2000), indicate a relatively strong influence of L_z/d. In Henderson (1997), for Re = 10^3; see also Henderson and Karniadakis (1995), a change from $L_z/d = 6.3$ to 25 resulted in a completely different appearance of the lift signal. The signal for $L_z/d = 25$ is strongly modulated in amplitude with occasional instances where the lift amplitude falls almost to zero. In the smaller domain, no such events are found. R.m.s. lift coefficients are not reported, due to transients and limitations in the simulation time period for each L_z/d. However, it is indicated from the lift-signal appearance for $L_z/d = 25$ that at least 100 mean shedding periods are needed to obtain reliable statistics. It is not possible, from

reported 3-D simulation studies so far, to provide any detailed guideline on the necessary spanwise length to effectively capture all significant flow features relevant for the fluctuating lift; see also Section 6.3.3.

References

Anagnostopoulos, P., 1994. Numerical investigation of response and wake characteristics of a vortex-excited cylinder in a uniform stream. Journal of Fluids and Structures 8, 367–390.

Anagnostopoulos, P., Iliadis, G., Richardson, S., 1996. Numerical study of the blockage effects on viscous flow past a circular cylinder. International Journal of Numerical Methods in Fluids 22, 1061–1074.

Apelt, C.J., West, G.S., 1996. Comparison of two methods for direct measurement of sectional fluctuating lift on a circular cylinder. Experiments in Fluids 20, 232–233.

Baban, F., So, R.M.C., Ötugen, M.V., 1989. Unsteady forces on circular cylinders in cross-flow. Experiments in Fluids 7, 293–302.

Baek, S.J., Sung, H.J., 1998. Numerical simulation of the flow behind a rotary oscillating circular cylinder. Physics of Fluids 10, 869–876.

Balachandar, S., Mittal, R., Najjar, F.M., 1997. Properties of the mean recirculation region in the wakes of two-dimensional bluff bodies. Journal of Fluid Mechanics 351, 167–199.

Barkley, D., Henderson, R.D., 1996. Three-dimensional Floquet stability analysis of the wake of a circular cylinder. Journal of Fluid Mechanics 322, 215–241.

Basu, R.I., 1985. Aerodynamic forces on structures of circular cross section, Part 1: model-scale data obtained under two-dimensional conditions in low-turbulence streams. Journal of Wind Engineering and Industrial Aerodynamics 21, 273–294.

Batcho, P., Karniadakis, G.E., 1991. Chaotic transport in two- and three-dimensional flow past a cylinder. Physics of Fluids A 3, 1051–1062.

Batham, J.P., 1973. Pressure distribution on circular cylinders at critical Reynolds numbers. Journal of Fluid Mechanics 57, 209–228.

Bays-Muchmore, B., Ahmed, A., 1993. On streamwise vortices in turbulent wakes of cylinders. Physics of Fluids A 5, 387–392.

Bearman, P.W., 1969. On vortex shedding from a circular cylinder in the critical Reynolds number regime. Journal of Fluid Mechanics 37, 577–585.

Bearman, P.W., Wadcock, A.J., 1973. The interaction between a pair of circular cylinders normal to a stream. Journal of Fluid Mechanics 61, 499–511.

Beaudan, P., Moin, P., 1994. Numerical experiments on the flow past a circular cylinder at sub-critical Reynolds number. Report No. TF-62, Thermosciences Division, Department of Mechanical Engineering, Stanford University.

Behr, M., Hastreiter, D., Mittal, S., Tezduyar, T.E., 1995. Incompressible flow past a circular cylinder: dependence of the computed flow field on the location of the lateral boundaries. Computer Methods in Applied Mechanics and Engineering 123, 309–316.

Behr, M., Liou, J., Shih, R., Tezduyar, T.E., 1991. Vorticity-streamfunction formulation of unsteady incompressible flow past a cylinder: sensitivity of computed flow field to the location of the outflow boundary. International Journal of Numerical Methods in Fluids 12, 323–342.

Bendat, J.S., Piersol, A.G., 1984. Random Data—Analysis and Measurement Procedures, 2nd edition. Wiley, New York.

Benson, M.G., Bellamy-Knights, P.G., Gerrard, J.H., Gladwell, I., 1989. A viscous splitting algorithm applied to low Reynolds number flows round a circular cylinder. Journal of Fluids and Structures 3, 439–479.

Bertagnolio, F., 1999. Solution of the incompressible Navier–Stokes equations on domains with one or several open boundaries. International Journal of Numerical Methods in Fluids 31, 1061–1085.

Bingham, H.H., Weimer, D.K., Griffith, W., 1952. The cylinder and semicylinder in subsonic flow. Technical Report TR II-13, Dept. Physics, Princeton University.

Bishop, R.E.D., Hassan, A.Y., 1964. The lift and drag forces on a circular cylinder in a flowing fluid. Proceedings Royal Society (London), Series A 277, 32–50.

Blackburn, H., Henderson, R., 1996. Lock-in behavior in simulated vortex-induced vibration. Experimental Thermal and Fluid Science 12, 184–189.

Blackburn, H.M., Melbourne, W.H., 1996. The effect of free-stream turbulence on sectional lift forces on a circular cylinder. Journal of Fluid Mechanics 306, 267–292.

Blackburn, H.M., Melbourne, W.H., 1997. Sectional lift forces for an oscillating circular cylinder in smooth and turbulent flows. Journal of Fluids and Structures 11, 413–432.

Blake, W.K., 1986. . Mechanics of Flow-Induced Sound and Vibration, Vol. 1. Academic Press, New York.

Blevins, R.D., 1990. Flow-Induced Vibration, 2nd edition, Van Nostrand Reinhold, New York.

Bloor, M.S., 1964. The transition to turbulence in the wake of a circular cylinder. Journal of Fluid Mechanics 19, 290–304.

Borthwick, A., 1986. Comparison between two finite-difference schemes for computing the flow around a cylinder. International Journal of Numerical Methods in Fluids 6, 275–290.

Bouak, F., Lemay, J., 1998. Passive control of the aerodynamic forces acting on a circular cylinder. Experimental Thermal and Fluid Science 16, 112–121.

Braza, M., Chassaing, P., Ha Minh, H., 1986. Numerical study and physical analysis of the pressure and velocity fields in the near wake of a circular cylinder. Journal of Fluid Mechanics 165, 79–130.

Brede, M., Eckelmann, H., Rockwell, D., 1996. On secondary vortices in the cylinder wake. Physics of Fluids 8, 2117–2124.

Breuer, M., 1998. Numerical and modeling influences on large eddy simulations for the flow past a circular cylinder. International Journal of Heat and Fluid Flow 19, 512–521.

Bruun, H.H., Davies, P.O.A.L., 1975. An experimental investigation of the unsteady pressure forces on a circular cylinder in a turbulent cross flow. Journal of Sound and Vibration 40, 535–559.

Bublitz, P., 1972. Unsteady pressures and forces acting on an oscillating circular cylinder in transverse flow. In: Naudascher, E. (Ed.), IUTAM-IAHR Flow-Induced Structural Vibrations. Symp. Karlsruhe. Springer, Berlin, pp. 443–453.

Bychov, N.M., Kovalenko, V.M., 1983. Aerodynamics of a circular cylinder in crossflow. Fluid Mechanics—Soviet Research 12, 1–16.

Chen, Y.N., 1971a. Fluctuating lift forces of the Karman vortex streets on single circular cylinders and in tube bundles. Part 1. The vortex street geometry of the single circular cylinder. ASME Paper No. 71-Vibr-11.

Chen, Y.N., 1971b. Fluctuating lift forces of the Karman vortex streets on single circular cylinders and in tube bundles. Part 2. Lift forces of single cylinders. ASME Paper No. 71-Vibr-12.

Cheng, C.H., Hong, J.L., Aung, W., 1997. Numerical prediction of lock-on effect on convective heat transfer from a transversely oscillating circular cylinder. International Journal of Heat and Mass Transfer 40, 1825–1834.

Cheung, J.C.K., Melbourne, W.H., 1983. Turbulence effects on some aerodynamic parameters of a circular cylinder at supercritical Reynolds numbers. Journal of Wind Engineering and Industrial Aerodynamics 14, 399–410.

Davies, M.E., 1976. A comparison of the wake structure of a stationary and oscillating bluff body, using a conditional averaging technique. Journal of Fluid Mechanics 75, 209–231.

Dougherty, N.S., Holt, J.B., Liu, B.L., O'Farrell, J.M., 1989. Time-accurate Navier–Stokes computations of unsteady flows: The Karman vortex street. In: 27th Aerospace Sciences Meeting, January 9–12, 1989/Reno, Nevada, AIAA Paper 89-0144, pp. 1–8.

Drescher, H., 1956. Messung der auf querangeströmte Zylinder ausgeübten zeitlich veränderten Drücke. Zeitschrift für Flugwissenschaften und Weltraumforschung 4, 17–21.

Dupin, P., Teissié-Solier, M., 1928. Les tourbillons alternés de Bénard–Karman. Revue Générale de l'Électricité 24, 53–60.

Engelman, M.S., Jamnia, M.A., 1990. Transient flow past a circular cylinder: a benchmark solution. International Journal of Numerical Methods in Fluids 11, 985–1000.

ESDU, 1985. Circular–cylindrical structures: dynamic response to vortex shedding, Part 1: calculation procedures and derivation, Item Number 85038. Engineering Sciences Data Unit (ESDU), ESDU International, 251–259 Regent Street, London W1R 7AD, UK.

Etkin, B., Korbacher, G.K., Keefe, R.T., 1956. Acoustic radiation from a stationary cylinder in a fluid stream (Aeolian tones) Report 39, Institute of Aerophysics, University of Toronto (UTIA).

Evangelinos, C., Karniadakis, G.E., 1999. Dynamics and flow structures in the turbulent wake of rigid and flexible cylinders subject to vortex-induced vibrations. Journal of Fluid Mechanics 400, 91–124.

Farell, C., 1981. Flow around fixed circular cylinders: fluctuating loads ASCE. Journal of the Engineering Mechanics Division 107, 565–587.

Farrant, T., Tan, M., Price, W.G., 2000. A cell boundary element method applied to laminar vortex-shedding from arrays of cylinders in various arrangements. Journal of Fluids and Structures 14, 375–402.

Feng, C.C., 1968. The measurement of vortex induced effects in flow past stationary and oscillating circular and D-section cylinders. M.A. Sc. Thesis, Department of Mechanical Engineering, The University of British Columbia.

Ferguson, N., Parkinson, G.V., 1967. Surface and wake flow phenomena of the vortex-excited oscillation of a circular cylinder. ASME Journal of Engineering for Industry 89, 831–838.

Fey, U., König, M., Eckelmann, H., 1998. A new Strouhal–Reynolds-number relationship for the circular cylinder in the range $47 < Re < 2 \times 10^5$. Physics of Fluids 10, 1547–1549.

Fox, T.A., West, G.S., 1990. On the use of end plates with circular cylinders. Experiments in Fluids 9, 237–239.

Franke, R., Rodi, W., Schönung, B., 1990. Numerical calculation of laminar vortex-shedding flow past cylinders. Journal of Wind Engineering and Industrial Aerodynamics 35, 237–257.

Fröhlich, J., Rodi, W., Kessler, P., Parpais, S., Bertoglio, J.P., Laurence, D., 1998. Large eddy simulation of flow around circular cylinders on structured and unstructured grids. In: Hirschel, E.H. (Ed.),, Notes on Numerical Fluid Mechanics, Vol. 66. Vieweg Verlag, Braunschweig, pp. 319–338.

Fujino, T., Takahei, T., Nakagawa, K., Arita, Y., 1958. The dynamic behavior of tall stacks under the action of wind. In: Proceedings 7th Japan National Congress for Applied Mechanics, University of Tokyo 1957, pp. 387–392.

Fung, Y.C., 1960. Fluctuating lift and drag acting on a cylinder in a flow at supercritical Reynolds numbers. Journal of the Aerospace Sciences 27, 801–814.

Gartshore, I.S., 1984. Some effects of upstream turbulence on the unsteady lift forces imposed on prismatic two dimensional bodies. ASME Journal of Fluids Engineering 106, 418–424.

Gerich, D., 1987. Über den kontinuerlich arbeitenden Rauchdraht und die Sichtbarmachung eines Übergangs vom laminaren zum turbulenten Nachlauf, Bericht 104/1987, Max-Planck-Institut für Strömungsforschung, Göttingen.

Gerrard, J.H., 1955. Measurements of the sound from circular cylinders in an air stream. Proceedings Physical Society, Section B 68, 453–461.

Gerrard, J.H., 1961. An experimental investigation of the oscillating lift and drag of a circular cylinder shedding turbulent vortices. Journal of Fluid Mechanics 11, 244–256.

Gerrard, J.H., 1965. A disturbance-sensitive Reynolds number range of the flow past a circular cylinder. Journal of Fluid Mechanics 22, 187–196.

Gerrard, J.H., 1978. The wakes of cylindrical bluff bodies at low Reynolds number. Philosophical Transactions of The Royal Society of London, Series A 288, 351–382.

Gerrard, J.H., 1997. Numerical study of the instabilities in the near wake of a circular cylinder at low Reynolds number. Journal of Fluids and Structures 11, 271–291.

Gharib, M.R., Leonard, A., Shiels, D.G., Roshko, A., Gharib, M., 1997. Exploration of flow-induced vibration at low mass and damping. In: ASME Fourth International Symposium on Fluid–Structure Interaction, Aeroelasticity, Flow-Induced Vibration and Noise, Dallas, November 16–21, 1997, ASME, New York, pp. 1–7.

Gresho, P.M., Chan, S.T., Lee, R.L., Upson, C.D., 1984. A modified finite element method for solving the time-dependent, incompressible Navier–Stokes equations. Part 2. International Journal of Numerical Methods in Fluids 4, 619–640.

Gunzburger, M.D., Lee, H.C., 1996. Feedback control of Karman vortex shedding. ASME Journal of Applied Mechanics 63, 828–835.

Hama, F.R., 1957. Three-dimensional vortex pattern behind a circular cylinder. Journal of the Aeronautical Sciences 24, 156–158.

Hanson, F.B., Richardson, P.D., 1968. The near-wake of a circular cylinder in crossflow. ASME Journal of Basic Engineering 90, 476–484.

He, X., Doolen, G.D., 1997. Lattice Boltzmann method on a curvilinear coordinate system: Vortex shedding behind a circular cylinder. Physical Review E 56, 434–440.

Henderson, R.D., 1997. Nonlinear dynamics and pattern formation in turbulent wake transition. Journal of Fluid Mechanics 352, 65–112.

Henderson, R.D., 1998. Turbulent wake transition. In: Bearman, P.W., Williamson, C.H.K. (Eds.), Advances in the Understanding of Bluff Body Wakes and Vortex-Induced Vibration. ASME, Washington D.C., New York.

Henderson, R.D., Karniadakis, G.E., 1995. Unstructured spectral element methods for simulation of turbulent flows. Journal of Computational Physics 122, 191–217.

Holle, W., 1938. Frequenz- und Schallstärkemessungen an Hiebtönen. Akustische Zeitschrift 3, 321–331.

Howell, J.F., Novak, M., 1979. Vortex shedding from circular cylinders in turbulent flow. In: Cermak, J.E. (Ed.), 5th International Conference on Wind Engineering, Fort Collins, Colorado, Pergamon, Oxford, pp. 619–629.

Humphreys, J.S., 1960. On a circular cylinder in a steady wind at transition Reynolds numbers. Journal of Fluid Mechanics 9, 603–612.

Huthloff, E., 1975. Windkanaluntersuchungen zur Bestimmung der periodischen Kräfte bei der Umströmung schlanker scharfkantiger Körper. Der Stahlbau 44, 97–103.

Hwang, R.R., Lin, S.H., 1992. On laminar wakes behind a circular cylinder in stratified fluids. ASME Journal of Fluids Engineering 114, 20–28.

Iida, A., Otaguro, T., Kato, C., Fujita, H., 1997. Prediction of aerodynamic sound spectra from a circular cylinder. In: S. of Instrument, C. E. of Japan (Eds.), Proceedings of the 5th Triennial International Symposium on Fluid Control, Measurement and Visualization (FLUCOME '97), Vol. 1. Hayama, Japan, 1–4 September, 1997, pp. 126–131.

Izumi, H., Taniguchi, N., Kawata, Y., Kobayashi, T., Adachi, T., 1994. Three-dimensional flow analysis around a circular cylinder (1st report, in case of a stationary circular cylinder). Transactions of JSME, Series B 60, 207–214. No. 94-0498.

Jameson, A., Martinelli, L., 1998. Mesh refinement and modeling errors in flow simulation. AIAA Journal 36, 676–686.

Jia, W., 1998. An accurate semi-Lagrangian scheme designed for incompressible Navier–Stokes equations written in generalized coordinates. Transactions of Japan Society of Aeronautical and Space Sciences 41, 105–117.

Jordan, S.K., Fromm, J.E., 1972. Oscillatory drag, lift, and torque on a cylinder in a uniform flow. Physics of Fluids 15, 371–376.

Kacker, S.C., Pennington, B., Hill, R.S., 1974. Fluctuating lift coefficient for a circular cylinder in cross flow. Journal Mechanical Engineering Science 16, 215–224.

Kalro, V., Tezduyar, T.E., 1997. Parallel 3D computation of unsteady flows around circular cylinders. Parallel Computing 23, 1235–1248.

Karniadakis, G.E., 1988. Numerical simulation of forced convection heat transfer from a cylinder in crossflow. International Journal of Heat and Mass Transfer 31, 107–118.

Kato, C., Ikegawa, M., 1991. Large eddy simulation of unsteady turbulent wake of a circular cylinder using the finite element method. In: Celik, I., Kobayashi, T., Ghi, K.N., Kurokawa, J. (Eds.),, Advances in Numerical Simulation of Turbulent Flows, FED-Vol. 117. ASME, New York, pp. 49–56.

Keefe, R.T., 1961. An investigation of the fluctuating forces acting on a stationary circular cylinder in a subsonic stream, and of the associated sound field. Report No. 76, Institute of Aerophysics, University of Toronto (UTIA).

Keefe, R.T., 1962. Investigation of the fluctuating forces on a stationary circular cylinder in a subsonic stream and of the associated sound field. The Journal of the Acoustical Society of America 34, 1711–1714.

Khalak, A., Williamson, C.H.K., 1996. Dynamics of a hydroelastic cylinder with very low mass and damping. Journal of Fluids and Structures 10, 455–472.

King, R., 1977. A review of vortex shedding research and its application. Ocean Engineering 4, 141–172.

Kiya, M., Suzuki, Y., Arie, M., Hagino, M., 1982. A contribution to the free-stream turbulence effect on the flow past a circular cylinder. Journal of Fluid Mechanics 115, 151–164.

Kiya, M., Tamura, H., 1989. Flow about a circular cylinder in and near a turbulent plane mixing layer. ASME Journal of Fluids Engineering 111, 124–129.

Kjellgren, P., 1997. A semi-implicit fractional step finite element method for viscous incompressible flows. Computational Mechanics 20, 541–550.

Kravchenko, A.G., Moin, P., 1998. B-spline methods and zonal grids for numerical simulations of turbulent flows. Report No. TF-73, Flow Physics and Computational Division, Department of Mechanical Engineering, Stanford University.

Kravchenko, A.G., Moin, P., Shariff, K., 1999. B-spline method and zonal grids for simulations of complex turbulent flows. Journal of Computational Physics 151, 757–789.

Kwon, K., Choi, H., 1996. Control of laminar vortex shedding behind a circular cylinder. Physics of Fluids 8, 479–486.

Lecointe, Y., Piquet, J., 1984. On the use of several compact methods for the study of unsteady incompressible viscous flow round a circular cylinder. Computers and Fluids 12, 255–280.

Lecointe, Y., Piquet, J., 1989. Flow structure in the wake of an oscillating cylinder. ASME Journal of Fluids Engineering 111, 139–148.

Lee, T., Basu, S., 1997. Nonintrusive measurements of the boundary layer developing on a single and two circular cylinders. Experiments in Fluids 23, 187–192.

Lee, T., Budwig, R., 1991. A study of the effect of aspect ratio on vortex shedding behind circular cylinders. Physics of Fluids A 3, 309–315.

Leehey, P., Hanson, C.E., 1971. Aeolian tones associated with resonated vibration. Journal of Sound and Vibration 13, 465–483.

Li, J., Chambarel, A., Donneaud, M., Martin, R., 1991. Numerical study of laminar flows past one and two circular cylinders. Computers and Fluids 19, 155–170.

Li, J., Sun, J., Roux, B., 1992. Numerical study of an oscillating cylinder in uniform flow and in the wake of an upstream cylinder. Journal of Fluid Mechanics 237, 457–478.

Lienhard, J.H., 1966. Synopsis of lift, drag, and vortex frequency data for rigid circular cylinders. Bulletin 300, Washington State University.

Lilek, Ž., Muzaferija, S., Perić, M., Seidl, V., 1997. Computation of unsteady flows using nonmatching blocks of structured grid. Numerical Heat Transfer, Part B 32, 403–418.

Lin, J.C., Vorobieff, P., Rockwell, D., 1996. Space-time imaging of a turbulent near-wake by high-image-density particle image cinematography. Physics of Fluids 8, 555–564.

Lin, S.Y., Wu, T.M., 1994. Flow control simulations around a circular cylinder by a finite volume method. Numerical Heat Transfer, Part A 26, 301–319.

Linke, W., 1931. Neue Messungen zur Aerodynamik des Zylinders, insbesondere seines reinen Reibungswiderstandes. Physikalische Zeitschrift 32, 900–914.

Liu, C., Zheng, X., Sung, C.H., 1998. Preconditioned multigrid methods for unsteady incompressible flows. Journal of Computational Physics 139, 35–57.

Loiseau, H., Szechenyi, E., 1972. Analyse expérimentale des portances sur un cylindre immobile soumis a un écoulement perpendiculaire a son axe a des nombres Reynolds élevés. La Recherche Aerospatiale 5, 279–291.

Lu, X., Dalton, C., Zhang, J., 1996. Application of large eddy simulation to an oscillating flow past a circular cylinder. In: Rodi, W., Bergles, G. (Eds.), Engineering Turbulence Modelling and Experiments 3. Elsevier Science, Oxford, pp. 187–197.

Lu, X., Dalton, C., Zhang, J., 1997a. Application of large eddy simulation to an oscillating flow past a circular cylinder. ASME Journal of Fluids Engineering 119, 519–525.

Lu, X., Dalton, C., Zhang, J., 1997b. Application of large eddy simulation to flow past a circular cylinder. ASME Journal of Offshore Mechanics and Arctic Engineering 119, 219–225.

Lu, X.Y., Dalton, C., 1996. Calculation of the timing of vortex formation from an oscillating cylinder. Journal of Fluids and Structures 10, 527–542.

Ma, X., Karamanos, G.S., Karniadakis, G.E., 2000. Dynamics and low-dimensionality of a turbulent wake. Journal of Fluid Mechanics 410, 29–65.

Macovsky, M.S., 1958. Vortex-induced vibration studies. Report 1190, Navy Department, David Taylor Model Basin, Hydromechanics Laboratory.

Mansy, H., Yang, P.M., Williams, D.R., 1994. Quantitative measurements of three-dimensional structures in the wake of a circular cylinder. Journal of Fluid Mechanics 270, 277–296.

Maskell, E.C., 1963. A theory of the blockage effects on bluff bodies and stalled wings in a closed wind tunnel. Reports and Memoranda No. 3400, Aeronautical Research Council (ARC).

McGregor, D.M., 1957. An experimental investigation of the oscillating pressures on a circular cylinder in a fluid stream. Technical Note 14, Institute of Aerophysics, University of Toronto (UTIA).

McGregor, D.M., Etkin, B.E., 1958. Investigation of the fluctuating pressures on a circular cylinder in an airstream. Physics of Fluids 1, 162–164.

Meneghini, J.R., Bearman, P.W., 1993. Numerical simulation of high amplitude oscillatory-flow about a circular cylinder using a discrete vortex method. In: Proc. AIAA Shear Flow Conference, Orlando, AIAA Paper 93-3288, pp. 1–11.

Miller, G.D., Williamson, C.H.K., 1994. Control of three-dimensional phase dynamics in a cylinder wake. Experiments in Fluids 18, 26–35.

Mittal, R., Balachandar, S., 1995. Effect of three-dimensionality on the lift and drag of nominally two-dimensional cylinders. Physics of Fluids 7, 1841–1865.

Moeller, M.J., 1982. Measurement of unsteady forces on a circular cylinder in cross flow at subcritical Reynolds numbers, Ph.D. Thesis, Massachusetts Institute of Technology, USA.

Moeller, M.J., Leehey, P., 1984. Unsteady forces on a cylinder in cross flow at subcritical Reynolds numbers. In: Païdoussis, M.P. Griffin, O.M., Sevik, M. (Eds.), ASME Symposium on Flow-Induced Vibrations, Vol. 1, New Orleans, 1984. ASME, New York, pp. 57–71.

Mohr, K.-H., 1981. Messungen instationären Drücke bei Queranströmung von Kreiszylindern unter Berücksichtigung fluidelastischer Effekte. Ph.D. Thesis, KFA Jülich GmbH, Germany. Report Jul-1732.

Morkovin, M.V., 1964. Flow around circular cylinder — a kaleidoscope of challenging fluid phenomena. In: Hansen, A.G. (Ed.), ASME Symposium on Fully Separated Flows. Philadelphia, ASME, New York, pp. 102–118.

Mulcahy, T.M., 1983. Measurement of crossflow forces on tubes. ASME Paper 83-PVP-77.

Mulcahy, T.M., 1984. Fluid forces on a rigid cylinder in turbulent crossflow. In: Païdoussis, M.P., Griffin, O.M., Sevik, M. (Eds.), ASME Symposium on Flow-Induced Vibrations, New Orleans, 1984, Vol. 1, ASME, New York, pp. 15–28.

Newman, D.J., Karniadakis, G.E., 1995. Direct numerical simulations of flow over a flexible cable. In: Bearman, P.W., (Ed.), Proceedings of the 6th International Conference on Flow-Induced Vibration, London/UK, 10–12 April 1995, Balkema, Rotterdam, pp. 193–203.

Newman, D.J., Karniadakis, G.E., 1996. Simulations of flow over a flexible cable: A comparison of forced and flow-induced vibration. Journal of Fluids and Structures 10, 439–454.

Noca, F., Shiels, D., Jeon, D., 1997. Measuring instantaneous fluid dynamic forces on bodies, using only velocity fields and their derivatives. Journal of Fluids and Structures 11, 345–350.

Noca, F., Shiels, D., Jeon, D., 1999. A comparison of methods for evaluating time-dependent fluid dynamic forces on bodies, using only velocity fields and their derivatives. Journal of Fluids and Structures 13, 551–578.

Norberg, C., 1986. Interaction between freestream turbulence and vortex shedding for a single tube in cross-flow. Journal of Wind Engineering and Industrial Aerodynamics 23, 501–514.

Norberg, C., 1987a. Effects of Reynolds number and a low-intensity freestream turbulence on the flow around a circular cylinder. Publ. 87/2, Dept. Applied Thermodynamics and Fluid Mechanics, Chalmers University of Technology, Gothenburg, Sweden.

Norberg, C., 1987b. Reynolds number and freestream turbulence effects on the flow and fluid forces for a circular cylinder in cross flow. Ph.D. Thesis, Chalmers University of Technology, Gothenburg, Sweden.

Norberg, C., 1989. An experimental study of the circular cylinder in cross flow: transition around $Re = 5000$. In: Ko, N.W.M., Kot, S.C. (Eds.), Proceedings of the Fourth Asian Congress of Fluid Mechanics, Suppl. Vol., University of Hong Kong.

Norberg, C., 1992. An experimental study of the flow around cylinders joined with a step in the diameter. In: Davis, M.R., Walker, G.J. (Eds.),, Proceedings of the 11th Australasian Fluid Mechanics Conference, Vol. 1. Hobart, Australia, pp. 507–510.

Norberg, C., 1993a. Pressure forces on a circular cylinder in cross flow. In: Eckelmann, H. Graham, J.M.R., Huerre, P., Monkewitz, P.A. (Eds.), Bluff-Body Wakes, Dynamics and Instabilities. Proceedings of IUTAM Symposium Göttingen, September, 1992, Springer, Berlin, pp. 275–278.

Norberg, C., 1993b. Flow around rectangular cylinders: pressure forces and wake frequencies. Journal of Wind Engineering and Industrial Aerodynamics 49, 187–196.

Norberg, C., 1994. An experimental investigation of the flow around a circular cylinder: influence of aspect ratio. Journal of Fluid Mechanics 258, 287–316.

Norberg, C., 1998. LDV-measurements in the near wake of a circular cylinder. In: Bearman, P.W., Williamson, C.H.K. (Eds.), Advances in the Understanding of Bluff Body Wakes and Vortex-Induced Vibration. Washington D.C. ASME, New York, pp. 1–12.

Norberg, C., Sundén, B., 1987. Turbulence and Reynolds number effects on the flow and fluid forces on a single cylinder in cross flow. Journal of Fluids and Structures 1, 337–357.

Novak, M., Tanaka, H., 1977. Pressure correlations on a vibrating cylinder. In: Eaton, K.J. (Ed.), Proceedings of the 4th International Conference on Wind Effects on Buildings and Structures, Heathrow, UK, 1975, Cambridge University Press, Cambridge, pp. 227–232.

Olinger, D.J., Alexandrou, A.N., 1998. Non-harmonic forcing of a cylinder wake by a periodic freestream flow. In: Bearman, P.W., Williamson, C.H.K. (Eds.), Advances in the Understanding of Bluff Body Wakes and Vortex-Induced Vibration. ASME, Washington D.C., New York.

Park, J., Kwon, K., Choi, H., 1998. Numerical solutions of flow past a circular cylinder at Reynolds numbers up to 160. KSME International Journal 12, 1200–1205.

Patnaik, B.S.V., Narayana, P.A.A., Seetharamu, K.N., 1999. Numerical simulation of vortex shedding past a circular cylinder under the influence of buoyancy. International Journal of Heat and Mass Transfer 42, 3495–3507.

Persillon, H., Braza, M., 1998. Physical analysis of the transition to turbulence in the wake of a circular cylinder by three-dimensional Navier–Stokes simulation. Journal of Fluid Mechanics 365, 23–88.

Phillips, O.M., 1956. The intensity of Aeolian tones. Journal of Fluid Mechanics 1, 607–624.

Piñol, S., Grau, F.X., 1998. Influence of the no-slip boundary condition on the prediction of drag, lift, and heat transfer coefficients in the flow past a 2-D cylinder. Numerical Heat Transfer, Part A 34, 313–330.

Posdziech, O., Grundmann, R., 2000. A systematic approach to the numerical calculation of fundamental quantities of the two-dimensional flow over a circular cylinder. Journal of Fluids and Structures 1–25. submitted.

Posdziech, O., Grundmann, R., 2001. Numerical simulation of the flow around an infinitely long circular cylinder in the transition regime. Theoretical and Computational Fluid Dynamics 15, 121–141.

Prasad, A., Williamson, C.H.K., 1997a. The instability of the shear layer separating from a bluff body. Journal of Fluid Mechanics 333, 375–402.

Prasad, A., Williamson, C.H.K., 1997b. Three-dimensional effects in turbulent bluff-body wakes Journal of Fluid Mechanics, 343.

Protos, A., Goldschmidt, V.W., Toebes, G.H., 1968. Hydroelastic forces on bluff cylinders. In: Symposium on Unsteady Flow, Philadelphia, ASME, New York, pp. 1–9.

Provansal, M., Mathis, C., Boyer, L., 1987. Bénard–von Kármán instability: transient and forced regimes. Journal of Fluid Mechanics 182, 1–22.

Ribeiro, J.L.D., 1991. Effects of surface roughness on the two-dimensional flow past circular cylinders II: fluctuating forces and pressures. Journal of Wind Engineering and Industrial Aerodynamics 37, 311–326.

Ribeiro, J.L.D., 1992. Fluctuating lift and its spanwise correlation on a circular cylinder in a smooth and in a turbulent flow: a critical review. Journal of Wind Engineering and Industrial Aerodynamics 40, 179–198.

Richter, A., Naudascher, E., 1976. Fluctuating forces on a rigid circular cylinder in confined flow. Journal of Fluid Mechanics 78, 561–576.

Rogers, S.E., Kwak, D., 1990. Upwind differencing scheme for the time-accurate incompressible Navier–Stokes equations. AIAA Journal 28, 253–262.

Rosenfeld, M., 1994. Grid refinement test of time-periodic flows over bluff bodies. Computers and Fluids 23, 693–709.

Roshko, A., 1954. On the development of turbulent wakes from vortex streets, NACA Report 1191, National Advisory Committee for Aeronautics, Washington D.C.

Roshko, A., 1993. Perspectives on bluff body aerodynamics. Journal of Wind Engineering and Industrial Aerodynamics 49, 79–100.

Sa, J.Y., Chang, K.S., 1991. Shedding patterns of the near-wake vortices behind a circular cylinder. International Journal of Numerical Methods in Fluids 12, 463–474.

Sakamoto, H., Haniu, H., 1994. Optimum suppression of fluid forces acting on a circular cylinder. ASME Journal of Fluids Engineering 116, 221–227.

Schewe, G., 1983. On the force fluctuations acting on a circular cylinder in crossflow from subcritical up to transcritical Reynolds numbers. Journal of Fluid Mechanics 133, 265–285.

Schmidt, L.V., 1965. Measurements of fluctuating air loads on a circular cylinder. Journal of Aircraft 2, 49–55.

Schumm, M., Berger, E., Monkewitz, P.A., 1994. Self-excited oscillations in the wake of two-dimensional bluff bodies and their control. Journal of Fluid Mechanics 271, 17–53.

Schwabe, M., 1935. Über Druckermittlung in der nichtstationären ebenen Strömung. Ingenieur-Archiv 6, 34–50.

Sin, V.K., So, R.M.C., 1987. Local force measurements on finite-span cylinders in a cross-flow. ASME Journal of Fluids Engineering 109, 136–143.

Skop, R.A., Balusubramanian, S., 1997. A new twist on an old model for vortex-excited vibrations. Journal of Fluids and Structures 11, 395–412.

Slaouti, A., Stansby, P.K., 1992. Flow around two circular cylinders by the random-vortex method. Journal of Fluids and Structures 6, 641–670.

Smith, R.A., Moon, W.T., Kao, T.W., 1972. Experiments on flow about a yawed circular cylinder. ASME Journal of Basic Engineering 94, 771–776.

Smith, S.L., Brebbia, C.A., 1977. Improved stability techniques for the solution of Navier–Stokes equations. Applied Mathematical Modelling 1, 226–234.

So, R.M.C., Savkar, S.D., 1981. Buffeting forces on rigid cylinders in cross flows. Journal of Fluid Mechanics 105, 397–425.

Sohankar, A., Davidson, L., Norberg, C., 1995. Numerical simulation of unsteady flow around a square two-dimensional cylinder. In: Bilger, R.W. (Ed.), 12th Australasian Fluid Mechanics Conference. Sydney, Australia, pp. 517–520.

Sohankar, A., Davidson, L., Norberg, C., 2000. Large eddy simulation of flow past a square cylinder: Comparison of different subgrid scale models. ASME Journal of Fluids Engineering 122, 39–47.

Sohankar, A., Norberg, C., Davidson, L., 1998. Low-Reynolds number flow around a square cylinder at incidence: Study of blockage, onset of vortex shedding and outlet boundary condition. International Journal of Numerical Methods in Fluids 26, 39–56.

Sohankar, A., Norberg, C., Davidson, L., 1999. Simulation of unsteady three-dimensional flow around a square cylinder at moderate Reynolds numbers. Physics of Fluids 11, 288–306.

Sonneville, P., 1973. Étude du champ de pressions fluctuantes à la surface d'un cylindre circulaire. C. R. Académie des Sciences Paris, Série A 277, 383–385.

Sonneville, P., 1976. Étude de la structure tridimensionelle des écoulements autour d'un cylindre circulaire, Bulletin de la Direction des Etudes et Recherches, Série A, No. 3 – 1976, Electricité de France.

Stansby, P.K., 1974. The effects of end plates on the base pressure coefficient of a circular cylinder. Aeronautical Journal 78, 36–37.

Stansby, P.K., Slaouti, A., 1993. Simulation of vortex shedding including blockage by the random-vortex and other methods. International Journal of Numerical Methods in Fluids 17, 1003–1013.

Su, M., Kang, Q., 1999. Large eddy simulation of the turbulent flow around a circular cylinder at sub-critical Reynolds numbers. ACTA Mechanica Sinica 31, 100–105.

Surry, D., 1969. The effect of high intensity turbulence on the aerodynamics of a rigid circular cylinder at subcritical Reynolds number. Report No. 142, Institute for Aerospace Studies, University of Toronto (UTIAS).

Surry, D., Stathopoulos, T., 1977/78. An experimental approach to the economical measurements of spatially averaged wind loads. Journal of Wind Engineering and Industrial Aerodynamics 2, 385–397.

Swanson, J.C., Spaulding, M.L., 1978. Three dimensional numerical model of vortex shedding from a circular cylinder. In: Symposium on Non-Steady Fluid Dynamics. ASME, New York, pp. 207–216.

Szepessy, S., 1993. On the control of circular cylinder flow by end plates. European Journal of Mechanics, B/Fluids 12, 217–244.

Szepessy, S., 1994. On the spanwise correlation of vortex shedding from a circular cylinder at high subcritical Reynolds number. Physics of Fluids 6, 2406–2416.

Szepessy, S., Bearman, P.W., 1992. Aspect ratio and end plate effects on vortex shedding from a circular cylinder. Journal of Fluid Mechanics 234, 191–217.

Szepessy, S., Bearman, P.W., 1993. Analysis of a pressure averaging device for measuring aerodynamic forces on a circular cylinder. Experiments in Fluids 16, 120–128.

Tabata, M., Fujima, S., 1991. An upwind finite element scheme for high-Reynolds-number flows. International Journal of Numerical Methods in Fluids 12, 305–322.

Tang, S., Aubry, N., 1997. On the symmetry breaking instability leading to vortex shedding. Physics of Fluids 9, 2550–2561.

Tanida, Y., Okajima, A., Watanabe, Y., 1973. Stability of a circular cylinder oscillating in uniform flow or in a wake. Journal of Fluid Mechanics 61, 769–784.

Taniguchi, S., Miyakoshi, K., 1990. Fluctuating fluid forces acting on a circular cylinder and interference with a plane wall Effects of boundary layer thickness. Experiments in Fluids 9, 197–204.

Tezduyar, T.E., Shih, R., 1991. Numerical experiments on downstream boundary of flow past cylinder. Journal of Engineering Mechanics 117, 854–871.

Toebes, G.H., 1969. The unsteady flow and wake near an oscillating cylinder. ASME Journal of Basic Engineering 91, 493–504.

Tunstall, M.J., 1970. Fluctuating pressures on circular cylinders in uniform and turbulent flows. Lab. Note RD/L/N 45/70, Central Electricity Research Laboratories (CERL).

Unal, M.F., Lin, J.C., Rockwell, D., 1997. Force prediction by PIV imaging: a momentum-based approach. Journal of Fluids and Structures 11, 965–971.

Unal, M.F., Rockwell, D., 1988. On vortex formation from a cylinder. Part 1. The initial instability. Journal of Fluid Mechanics 190, 491–512.

van Nunen, J.W.G., Persoon, A.J., Tijdeman, H., 1972. Analysis of steady and unsteady pressure and force measurements on a circular cylinder at Reynolds numbers up to 7.7×10^6. NLR TR 69102 U, National Aerospace Laboratory, The Netherlands.

Vickery, B.J., 1966. Fluctuating lift and drag on a long cylinder of square cross-section in a turbulent stream. Journal of Fluid Mechanics 25, 481–494.

Vickery, B.J., Basu, R.I., 1983. Across-wind vibrations of structures of circular cross-section. Part 1: development of a mathematical model for two-dimensional conditions. Journal of Wind Engineering and Industrial Aerodynamics 12, 49–73.

Visbal, M.R., Gaitonde, D.V., 1999. High-order-accurate methods for complex unsteady subsonic flows. AIAA Journal 37, 1231–1239.

Watanabe, H., Ihara, A., Hashimoto, H., 1996. Hydraulic characteristics of a circular cylinder with a permeable wall. JSME International Journal, Series B 39, 482–488.

Weaver Jr., W., 1961. Wind-induced vibrations in antenna members. ASCE Journal of the Engineering Mechanics Division 87, 141–165.

West, G.S., Apelt, C.J., 1982. The effects of tunnel blockage and aspect ratio on the mean flow past a circular cylinder with Reynolds numbers between 10^4 and 10^5. Journal of Fluid Mechanics 114, 361–377.

West, G.S., Apelt, C.J., 1993. Measurements of fluctuating pressures and forces on a circular cylinder in the Reynolds number range 10^4 to 2.5×10^5. Journal of Fluids and Structures 7, 227–244.

West, G.S., Apelt, C.J., 1997. Fluctuating lift and drag forces on finite lengths of a circular cylinder in the subcritical Reynolds number range. Journal of Fluids and Structures 11, 135–158.

Williamson, C.H.K., 1988a. Defining a universal and continuous Strouhal–Reynolds number relationship for the laminar vortex shedding of a circular cylinder. Physics of Fluids 31, 2742–2744.

Williamson, C.H.K., 1988b. The existence of two stages in the transition to three-dimensionality of a cylinder wake. Physics of Fluids 31, 3165–3168.

Williamson, C.H.K., 1989. Oblique and parallel modes of vortex shedding in the wake of a circular cylinder at low Reynolds numbers. Journal of Fluid Mechanics 206, 579–627.

Williamson, C.H.K., 1992. The natural and forced formation of spot-like "vortex dislocations" in the transition of a wake. Journal of Fluid Mechanics 243, 393–441.

Williamson, C.H.K., 1996a. Vortex dynamics in the cylinder wake. Annual Review of Fluid Mechanics 28, 477–539.

Williamson, C.H.K., 1996b. Three-dimensional wake transition. Journal of Fluid Mechanics 328, 345–407.

Williamson, C.H.K., Brown, G.L., 1998. A series in $1/\sqrt{\mathrm{Re}}$ to represent the Strouhal–Reynolds number relationship of the cylinder wake. Journal of Fluids and Structures 12, 1073–1085.

Williamson, C.H.K., Roshko, A., 1990. Measurements of base pressure in the wake of a cylinder at low Reynolds numbers. Zeitschrift für Flugwissenschaften und Weltraumforschung 14, 38–46.

Wu, J., Sheridan, J., Welsh, M.C., Hourigan, K., 1996. Three-dimensional vortex structures in a cylinder wake. Journal of Fluid Mechanics 312, 201–222.

Yokoi, Y., Kamemoto, K., 1992. Initial stage of a three-dimensional vortex structure existing in a two-dimensional boundary layer separation flow (Observation of laminar boundary layer separation over a circular cylinder by flow visualization). JSME International Journal, Series II 35, 189–195.

Yokoi, Y., Kamemoto, K., 1993. Initial stage of a three-dimensional vortex structure existing in a two-dimensional boundary layer separation flow (Visual observation of laminar boundary layer separation over a circular cylinder from the side of a separated region). JSME International Journal, Series B 36, 201–206.

Zhang, H.Q., Fey, U., Noack, B.R., König, M., Eckelmann, H., 1995. On the transition of the cylinder wake. Physics of Fluids 7, 779–793.

Zhang, J., Dalton, C., 1997. Interaction of a steady approach flow and a circular cylinder undergoing forced oscillation. ASME Journal of Fluids Engineering 119, 808–813.

Zhang, J., Dalton, C., 1998. A three-dimensional simulation of a steady approach flow past a circular cylinder at low Reynolds number. International Journal of Numerical Methods in Fluids 26, 1003–1022.

Zhou, C.Y., So, R.M.C., Lam, K., 1999. Vortex-induced vibrations of an elastic circular cylinder. Journal of Fluids and Structures 13, 165–189.